Cenozoic evolution of the eastern Pamir: Implications for strain-accommodation mechanisms at the western end of the Himalayan-Tibetan orogen

Alexander C. Robinson[†]
An Yin[‡]
Craig E. Manning[§]
T. Mark Harrison[#]
Department of Earth and Space Sciences, University of California, Los Angeles, California 90095-1567, USA

Shuan-Hong Zhang[††]
Xiao-Feng Wang[‡‡]
Institute of Geomechanics, Chinese Academy of Geological Sciences, Beijing 100081, People's Republic of China

ABSTRACT

Detailed field mapping, geochronologic and thermochronologic analyses, and petrologic investigations conducted along the southern segment of the late Cenozoic Kongur Shan extensional system provide new information on the Cenozoic tectonic evolution of the eastern Pamir at the western end of the Himalayan-Tibetan orogen. Field relations and cooling-age patterns in the hanging wall and footwall of the active faults show a southward decrease in the magnitude of east-west extension along the southern Kongur Shan extensional system, from 20 km or less along the Muztaghata massif in the north, to <3 km along the Tashkorgan fault in the south. These results, in conjunction with previously published work on the northern segment of the Kongur Shan extensional system, show a general southward decrease in east-west extension along the entire length of the extensional system, consistent with models of extension primarily driven by oroclinal bending or radial thrusting of the Pamir. Petrologic data, $^{40}Ar/^{39}Ar$ cooling ages, and monazite Th-Pb ages from schists and gneisses in the footwall of the southern Kongur Shan normal fault along the Muztaghata massif record two tectonic events that immediately preceded late Miocene initiation of east-west extension: (1) high-grade schists and gneisses experienced upper amphibolite facies metamorphic conditions (9–10 kbar, 700–750 °C) dated as late Oligocene to middle Miocene by in situ ion-microprobe analyses of monazite inclusions in garnet; and (2) high-grade schists and gneisses were subsequently rapidly exhumed to shallow crustal levels in the late Miocene with $^{40}Ar/^{39}Ar$ biotite cooling ages of 7.5–9 Ma. Rapid exhumation was accommodated in part by the east-west–striking, south-dipping, Shen-ti normal fault. Field relations and regional geologic correlations indicate that this exhumation event was related to the formation of the Central Pamir gneiss domes, and the antiformal Muztaghata massif is the eastward continuation of the Sares dome of the Central Pamir. These observations suggest that the antiformal gneiss domes of the Central Pamir have not been offset across the Karakorum right-slip fault from the Qiangtang anticlinorium in Tibet. Instead, we propose that the development of the Central Pamir gneiss domes may have been related to Oligocene-Miocene northward underthrusting and thickening of crust beneath the Pamir.

Keywords: Pamir, extension, gneiss dome, geochronology, metamorphism, Karakorum.

INTRODUCTION

While knowledge of the tectonic history of the Tibetan Plateau has substantially improved in recent years (e.g., Matte et al., 1996; Murphy et al., 1997; Horton et al., 2002; Haines et al., 2003; Kapp et al., 2003a, 2003b; Taylor et al., 2003; Chung et al., 2005; Spurlin et al., 2005; Leier et al., 2007), the evolution of the northwestern portion of the Himalayan-Tibetan orogen, especially within the Pamir (Fig. 1), is relatively poorly understood. One of the more difficult problems has been determining the correct correlation of tectonic terranes between the Tibetan Plateau to the east and the Pamir–western Himalayan syntaxis region to the west (e.g., Schwab et al., 2004) due in part to political borders, difficult access over high-altitude terrane, and a lack of clear offset geologic markers. This problem has hindered our ability to determine (1) the magnitude of lateral offset along Cenozoic right-lateral Karakorum fault and its role in lateral extrusion tectonics (e.g., Peltzer and Tapponnier, 1988; Searle, 1996; Searle et al., 1998; Lacassin et al., 2004; Schwab et al., 2004), and (2) whether the asymmetry of the India-Asian collision zone is primarily the result of eastward lateral extrusion, along-strike variations in the distribution of shortening, or thrust system geometry (e.g., Tapponnier et al., 1982; Peltzer and Tapponnier, 1988; Houseman and England, 1996; Neil and Houseman, 1997; Cowgill et al., 2003). Our field and analytical results along the southern end of the Kongur Shan extensional system suggest that structural features of the Central Pamir terrane, the Muskol-Sares domes, continue across the north-striking Cenozoic Kongur Shan extensional system and have not been offset from the Qiangtang anticlinorium along the Karakorum fault.

[†]Present address: Department of Geosciences, University of Houston, Houston, Texas 77204, USA; acrobinson@uh.edu.
[‡]E-mail: yin@ess.ucla.edu.
[§]E-mail: manning@ess.ucla.edu.
[#]E-mail: tmh@argon.ess.ucla.edu.
[††]E-mail: zhangshuanhong@sina.com.
[‡‡]E-mail: wxf@cags.net.cn.

GSA Bulletin; July/August 2007; v. 119; no. 7/8; p. 882–896; doi: 10.1130/B25981.1; 12 figures; 1 insert; Data Repository item 2007134.

REGIONAL GEOLOGY

Tectonic Divisions

Understanding of the Cenozoic deformation history of the Pamir requires knowledge of both the original distribution of markers prior to the India-Asia collision and the mode of deformation during the collision. The western Himalayan-Tibetan orogen is composed of several distinctive terranes that evolved along, or were accreted to, the southern margin of Asia during the late Paleozoic–Mesozoic closure of the Tethys Ocean (e.g., Tapponnier et al., 1981; Şengör and Okurogullari, 1991; Burtman and Molnar, 1993; Hsu et al., 1995; Pan and Bian, 1996; Şengör and Natal'in, 1996; Yin and Harrison, 2000; Xiao et al., 2002; Schwab et al., 2004) (Figs. 1 and 2). While these terranes are generally interpreted as along-strike equivalents of terranes in central and eastern Tibet to the east and Afghanistan to the west (Tapponnier et al., 1981; Burtman and Molnar, 1993; Yin and Nie, 1996; Gaetani, 1997; Schwab et al., 2004), the correlation of these terranes is a subject of considerable debate. One interpretation is the South Pamir–Karakorum–Hindu Kush terrane correlates to the Qiangtang terrane of Tibet (Fig. 1) (e.g., Yin and Harrison, 2000), and this is supported by interpreted low magnitudes of right-lateral strike-slip motion along the southern Karakorum fault of 60–150 km (Searle, 1996; Searle et al., 1998; Murphy et al., 2000). A competing interpretation is that the Qiangtang and Lhasa terranes are equivalent to the Central Pamir and South Pamir–Karakorum–Hindu Kush, respectively, implying hundreds of kilometers of right slip along the Karakorum fault (Lacassin et al., 2004; Schwab et al., 2004). The latter is supported in part by correlation of similar-age magmatic belts and an anticlinorium in the Central Pamir, which includes the Muskol and Sares domes, that is interpreted to be equivalent to the Qiangtang anticlinorium (Schwab et al., 2004).

Cenozoic Tectonic Framework

The western Himalayan-Tibetan orogen is bounded in the north by the south-dipping Main Pamir thrust and thrusts of the Western Kunlun Shan (Figs. 1 and 2). The Main Pamir thrust has been interpreted to have accommodated ~300 km of southward subduction of crust of the Tarim-Tajik Basins during the Cenozoic (Burtman and Molnar, 1993; Thomas et al., 1994). Initiation age of slip along the Main Pamir thrust is considered to be either late Oligocene (Thomas et al., 1994, 1996; Sobel and Dumitru, 1997) or middle Eocene (Yin et al., 2002). In addition to overthrusting of the Pamir along the Main Pamir thrust, the region has also been internally shortened by 340 km along thrusts including the Tanymas and Pshart fault zones (Fig. 2) (Burtman and Molnar, 1993; Waldhör et al., 2001). However, the timing of this shortening is not well determined, and much of it could be pre-Cenozoic in age.

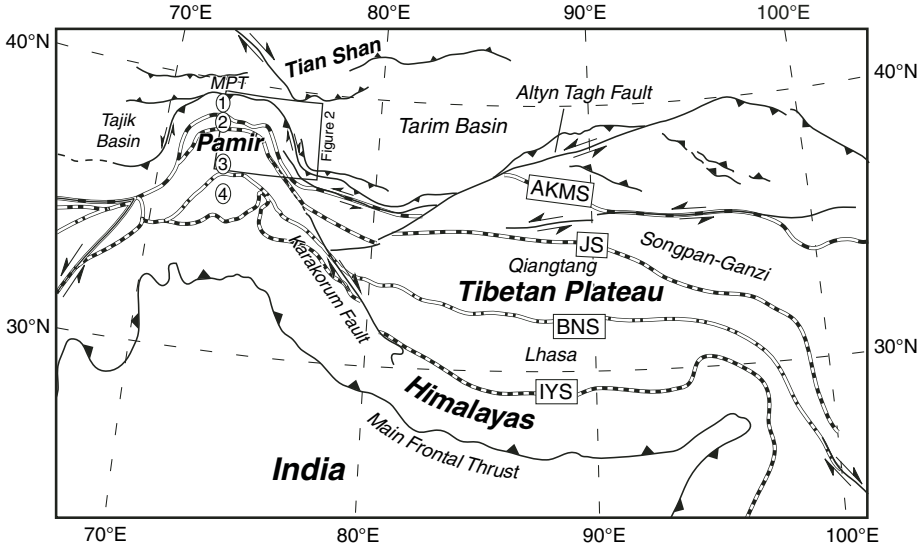

Figure 1. Simplified tectonic map of the Indo-Asian collision zone showing major active structures and suture zones (after Burtman and Molnar, 1993; Yin and Harrison, 2000). MPT—Main Pamir thrust; IYS—Indus-Yalu suture; BNS—Bangong-Nujiang suture; JS—Jinsha suture; AKMS—Ayimaqin-Kunlun-Mutztagh suture. Terranes of the western Indo-Asian collision zone are: 1—Northern Pamir; 2—Central Pamir; 3—South Pamir–Karakorum–Hindu Kush; 4—Kohistan arc.

Active deformation in the Pamir is dominated by east-west extension along the 250-km-long Kongur Shan extensional system in the east (Arnaud et al., 1993; Brunel et al., 1994; Robinson et al., 2004) and the Karakul rift in the west (Strecker et al., 1995; Blisniuk and Strecker, 1996) (Figs. 2 and 3). Age constraints from the northern Kongur Shan system indicate initiation of extension at 7–8 Ma (Robinson et al., 2004). Three kinematic models have been proposed to explain the active extension in the Pamir: (1) topographic collapse of the eastern Pamir during growth of the Kongur Shan and Muztaghata gneiss domes over a crustal-scale thrust ramp (Brunel et al., 1994), (2) radial thrusting along the Main Pamir thrust and/or oroclinal bending of the Pamir salient (Strecker et al., 1995; Yin et al., 2001), and (3) a transtensional bend in the right-slip Karakorum fault, linking late Cenozoic extension in the Pamir with extensional structures in southwest Tibet (Ratschbacher et al., 1994; Murphy et al., 2000). However, our previously published work along the Kongur Shan extensional system (and observations presented here) argues against any kinematic link with the Karakorum fault to the south (Robinson et al., 2004).

Active internal deformation within the Pamir also occurs along a series of northwest-striking right-slip faults in the southeastern Pamir region (e.g., the Aksu-Murgab and East Pamir faults; Fig. 2), which have been interpreted to link with the Karakorum fault to the south (Strecker et al., 1995). Slip rates on these structures are estimated to be <1 mm/yr, indicating that, aside from the extensional structures, active internal deformation of the Pamir is limited.

Central Pamir Gneiss Domes

Within the Central Pamir terrane, fault-bounded high-grade schists and gneisses with Miocene cooling ages are exposed in the cores of the east-west–trending Muskol and Sares antiforms (Pashkov and Dmitriyev, 1982; Peykre et al., 1982; Schwab et al., 2004) (Fig. 2), which we refer to as the Central Pamir gneiss domes. The metamorphic cores experienced greenschist to upper amphibolite facies metamorphic conditions and locally preserve migmatitic textures inferred to be Cenozoic in age (Pashkov and Dmitriyev, 1982; Schwab et al., 2004). Schwab et al. (2004) interpreted the eastern margin of the Sares dome to be truncated by the Karakorum fault, where the antiformal structures represent the offset westward continuation of the Qiangtang anticlinorium (Kapp et al., 2000; Yin

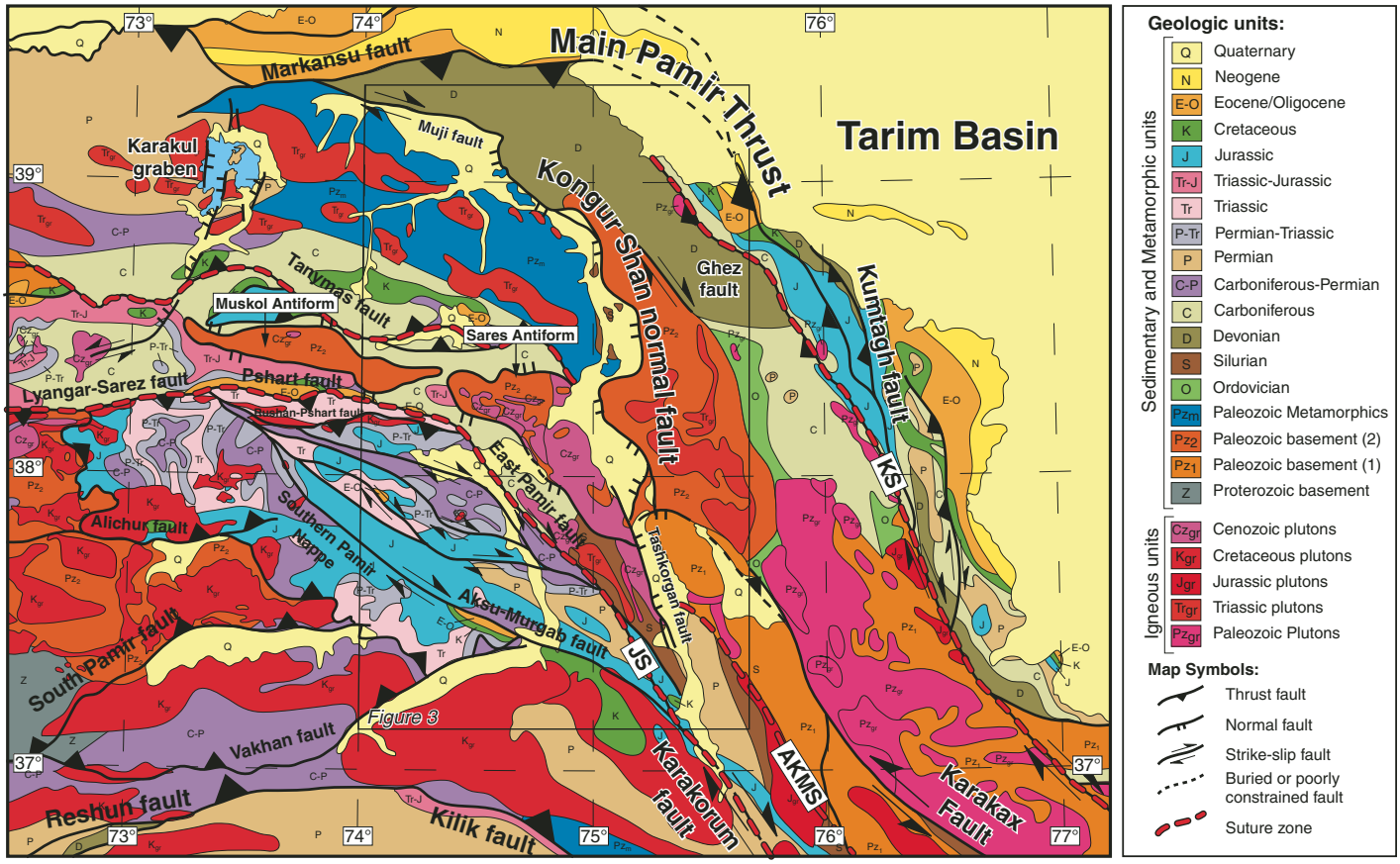

Figure 2. Simplified geologic map of the eastern Pamir, northern Karakoram, and Western Kunlun Shan showing distribution of lithologic ages and Cenozoic faults (after Yin and Bian, 1992; Strecker et al., 1995; Sobel and Dumitru, 1997; Robinson et al., 2004; Schwab et al., 2004). KS—Kudi suture; AKMS—Ayimaqin-Kunlun-Mutztagh suture; JS—Jinsha suture.

and Harrison, 2000), yielding ~200 km of offset along the northern Karakorum fault.

LITHOLOGIES OF THE SOUTHERN KONGUR SHAN REGION

Sedimentary Rocks

Paleozoic and Mesozoic Units

The southern end of the Tashkorgan Valley exposes a sequence of Permian limestones and slates (Liu, 1988; Yin and Bian, 1992) (Figs. 3 and 4[1]). The sequence consists of structurally higher limestones interlayered with minor slate and sandstone, (P_l), which overlie a thick slate unit (P_{sl}) that dips moderately to the northeast. Along the western side of the valley, Permian units are juxtaposed across a north-striking fault against a thick sequence of Triassic-Jurassic limestone (J_{l1} and J_{l2}) unconformably overlain by Cretaceous red beds (K_{ss}) that are folded into a northwest-trending syncline (Figs. 3 and 4) (Liu, 1988; Yin and Bian, 1992).

Quaternary Units

Quaternary units along the Kongur Shan extensional system consist dominantly of alluvial and fluvial deposits (Q_1 and Q_2; Figs. 3 and 4) and glacial moraine deposits (Q_m). Fine-grained lacustrine deposits of inferred Quaternary age are exposed sporadically along the northern end of the Tashkorgan Valley, possibly deposited while the outlet of the valley was dammed during a glacial maximum. Fine-grained deposits drape the western side of the Tashkorgan Valley at the southern end of the Tashkorgan fault (Q_l), and they are interpreted to be loess deposits. While these are inferred to be Quaternary, no age constraints are available.

Igneous Rocks

Igneous units along the southern end of the Kongur Shan extensional system consist of two primary groups (Fig. 3): (1) Triassic to Early Jurassic granites and granodiorites that intrude high-grade metasedimentary rocks and gneisses in the hanging wall and footwall of the Kongur Shan normal fault, and (2) Cenozoic plutons of the Tashkorgan igneous complex (Zhang et al., 1996) exposed along the western side of the central Tashkorgan Valley.

Mesozoic Units

Triassic to Early Jurassic granites and granodiorites (Mz_{gr}) consist of medium-grained bodies ranging in size from sills several meters in thickness to regionally extensive plutons. Plutons within the hanging wall of the Kongur Shan normal fault intrude upper amphibolite schists (Pz_{sch1}) and are unfoliated to weakly foliated (Robinson et al., 2004). Footwall plutons are exposed primarily within the core of the Muztaghata massif and intrude quartzofeldspathic gneisses (Pz_{gn1}) (Liu, 1988; Yin and Bian, 1992). Granitic rocks are weakly foliated along the southeastern side of the Muztaghata massif, but are strongly foliated with mylonitic fabrics to the northeast of the massif. U-Pb zircon

[1]Figures 4 and 5 are on a separate insert accompanying this issue.

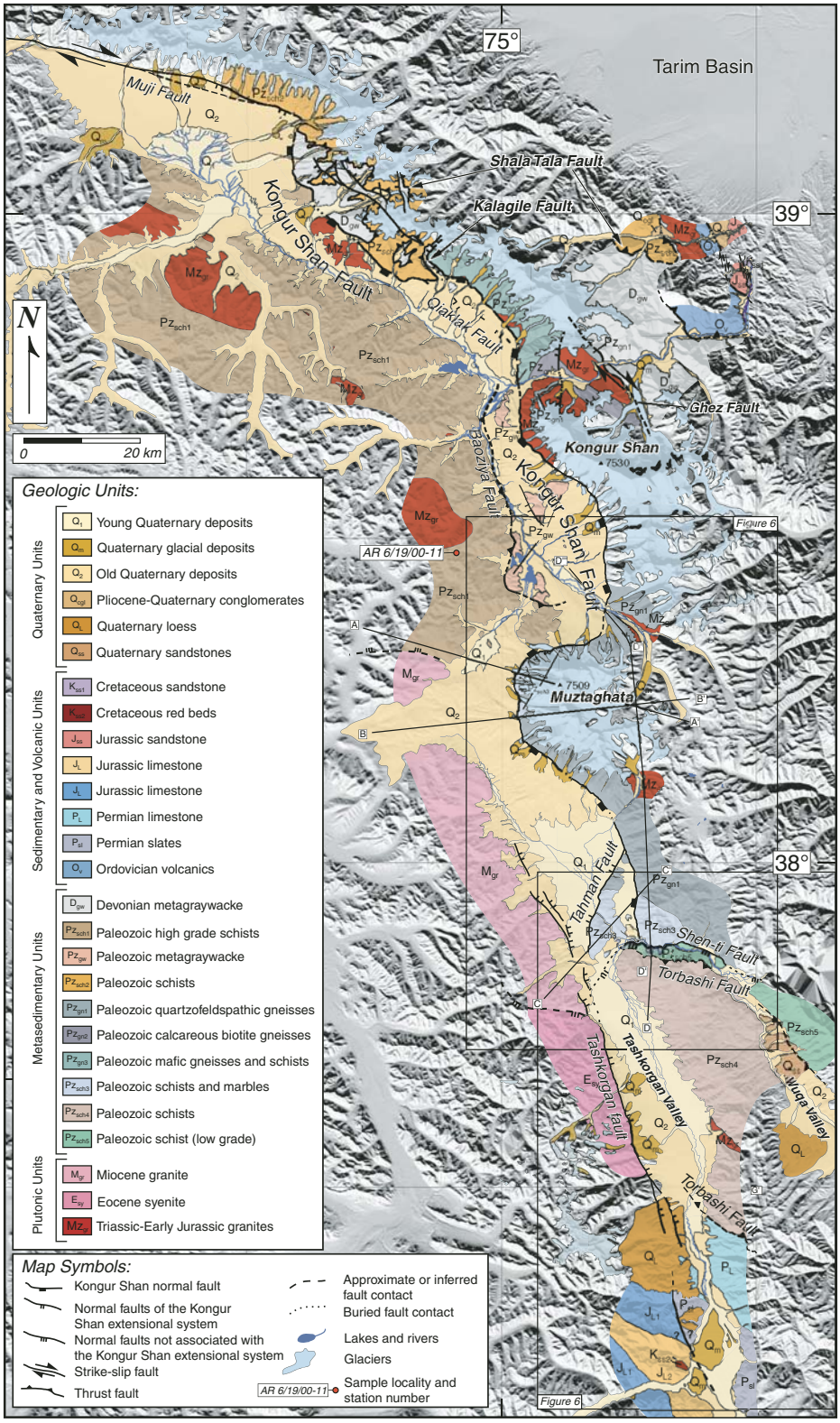

Figure 3. Geologic map of the Kongur Shan extensional system. For cross sections, see Figure 6.

dating of plutons in the hanging wall (Robinson et al., 2004) and the footwall (Xu et al., 1996; Robinson et al., 2004) has yielded ages of 230–199 Ma, consistent with previous age assignments to the late Paleozoic–early Mesozoic South Kunlun plutonic belt (Pan, 1992; Youngun and Hsu, 1994; Matte et al., 1996; Xu et al., 1996; Cowgill et al., 2003).

Cenozoic Units

Cenozoic plutons of the Tashkorgan alkaline complex are exposed for ~60 km along the western side of the Tashkorgan Valley (E_{sy} and M_{gr}; Figs. 3, 4, and 5 [see footnote 1]) (Zhang et al., 1996). They intrude high-grade metamorphic rocks of inferred Permian age to the west (Zhang et al., 1996) and are covered by Quaternary deposits or cut by the Tashkorgan normal fault to the east. The Tashkorgan alkaline complex consists of three rock types with progressively younger ages (Xu et al., 1996; Zhang et al., 1996): a medium-grained diopside syenite (E_{sy}), (K-feldspar $^{40}Ar/^{39}Ar$ age: 52.0 ± 0.7 Ma), a coarse-grained granite that intrudes the syenite (K-feldspar $^{40}Ar/^{39}Ar$ age: 18.2 Ma), and a biotite granite (M_{gr}) exposed along the northern end of the complex (biotite $^{40}Ar/^{39}Ar$ age: 11.45 ± 0.30 Ma; K-feldspar $^{40}Ar/^{39}Ar$ age: 11.58 ± 0.76 Ma). Geochemical analyses from all members of the Tashkorgan igneous complex suggest a high contribution of crustal material with Sr concentrations of 1000–3500 ppm (Zhang et al., 1996; Table DR1[2]), and $^{87}Sr/^{86}Sr$ ratios of 0.7094–0.7100 (Zhang et al., 1996).

Metamorphic Rocks

Hanging Wall of Kongur Shan Normal Fault

The hanging wall of the Kongur Shan fault consists of two metasedimentary units separated by the Baoziya thrust (Figs. 3 and 5) (Robinson et al., 2004): the structurally higher Pz_{sch1}, and the structurally lower Pz_{gw}. Pz_{sch1} is composed of pelitic schist, quartzite, and minor amphibolite. Typical mineral assemblages in the pelitic units yield upper amphibolite facies assemblages of quartz + plagioclase + biotite + garnet ± muscovite ± sillimanite ± K-feldspar. Previous studies along the northern portion of the hanging wall have shown that the unit is part of the Late Triassic medium- to high-grade, high-temperature and low-pressure metamorphic terrane, which developed during Triassic-Jurassic regional igneous activity (Robinson et al., 2004). While the northern portion of the hanging-wall

[2]GSA Data Repository item 2007134, Tables DR1–DR5 and Figures DR1–DR5, is available on the Web at http://www.geosociety.org/pubs/ft2007.htm. Requests may also be sent to editing@geosociety.org.

metamorphic sequence exhibits a distinct east-southeastward increase in metamorphic grade, the southern portion is uniformly amphibolite facies. Pz_{gw} is composed of light-green quartz-rich chloritic and calcareous schists, with minor layers of marble and dark-gray schist. Typical schist assemblages include quartz + white mica + calcite ± chlorite, indicating greenschist facies metamorphic conditions.

Footwall of the Kongur Shan and Tahman Normal Faults

High-grade metamorphic rocks in the footwall of the Kongur Shan and Tahman normal faults are composed of two main units: a structurally lower unit of quartzofeldspathic gneisses (Pz_{gn1}) and a structurally higher metasedimentary unit (Pz_{sch3}) (Figs. 3, 5, and 6). The gneiss unit exhibits well-developed compositional banding (Fig. 7A) with assemblages of quartz + plagioclase + biotite ± hornblende ± garnet ± K-feldspar (Fig. 8A). The overlying Pz_{sch3} is tens of meters thick along the western flank of the Muztaghata massif, but it is at least 10 km thick south of Muztaghata (Figs. 5 and 6C). Pz_{sch3} is composed of interlayered pelitic schist, mafic schist, marble, and calc-silicate. Pelitic schists in the footwall of the Kongur Shan and Tahman normal faults preserve primary metamorphic assemblages of quartz + biotite + kyanite + garnet + plagioclase + K-feldspar within the structurally deepest levels (Fig. 8B). Trace fibrolitic sillimanite is often observed in kyanite-bearing samples, but it becomes more abundant at higher structural levels along with the appearance of muscovite. Migmatitic textures are common in the basal part of the pelitic schists, indicating widespread partial melting through muscovite dehydration (Fig. 7B). Thermobarometric calculations from electron microprobe analyses of a garnet-kyanite-K-feldspar–bearing schist yield peak metamorphic conditions of 9–10 kbar, 700–750 °C (Table DR2, Fig. DR1, see footnote 1) using GRAIL (Garnet-Rutile-Illmenite-Al_2SiO_5-Quartz) and GASP (Garnet-Plagioclase-Quartz-Al_2SiO_5) equilibria (Bohlen and Liotta, 1986; Koziol and Newton, 1988), garnet-biotite Fe-Mg exchange, and THERMOCALC 2.7 (Powell et al., 1998). The calculated peak metamorphic conditions are consistent with the presence of metamorphic K-feldspar, kyanite, and migmatitic textures. As kyanite is the aluminosilicate phase coexisting with K-feldspar in many samples, partial melting appears to have begun during peak metamorphic conditions rather than during exhumation.

Hanging Wall of Tashkorgan Normal Fault

Along the east-flowing portion of the Tashkorgan River, upper amphibolite facies

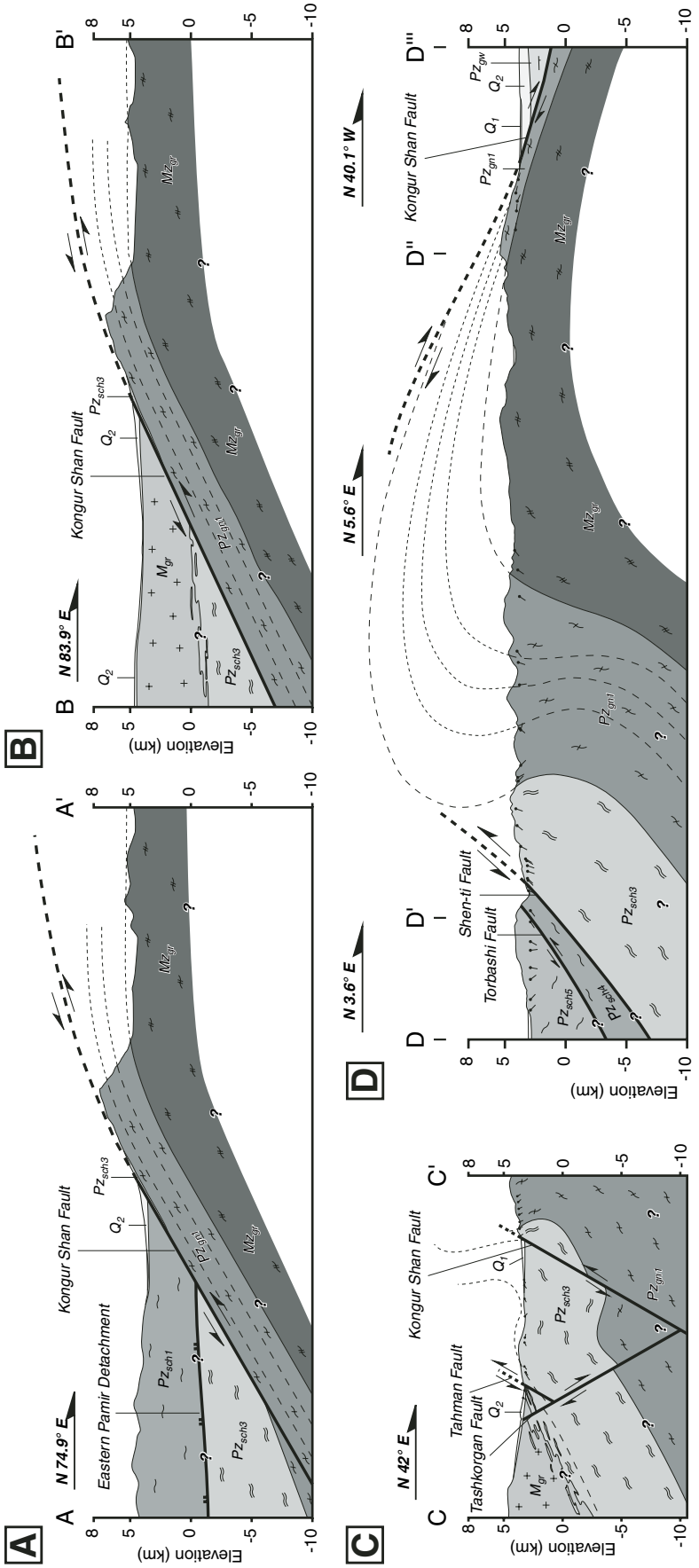

Figure 6. Geologic cross sections from Figure 3. (A) Cross section along A–A′. (B) Cross section along B–B′. (C) Cross section along C–C′. (D) Cross section along D–D′–D″–D‴.

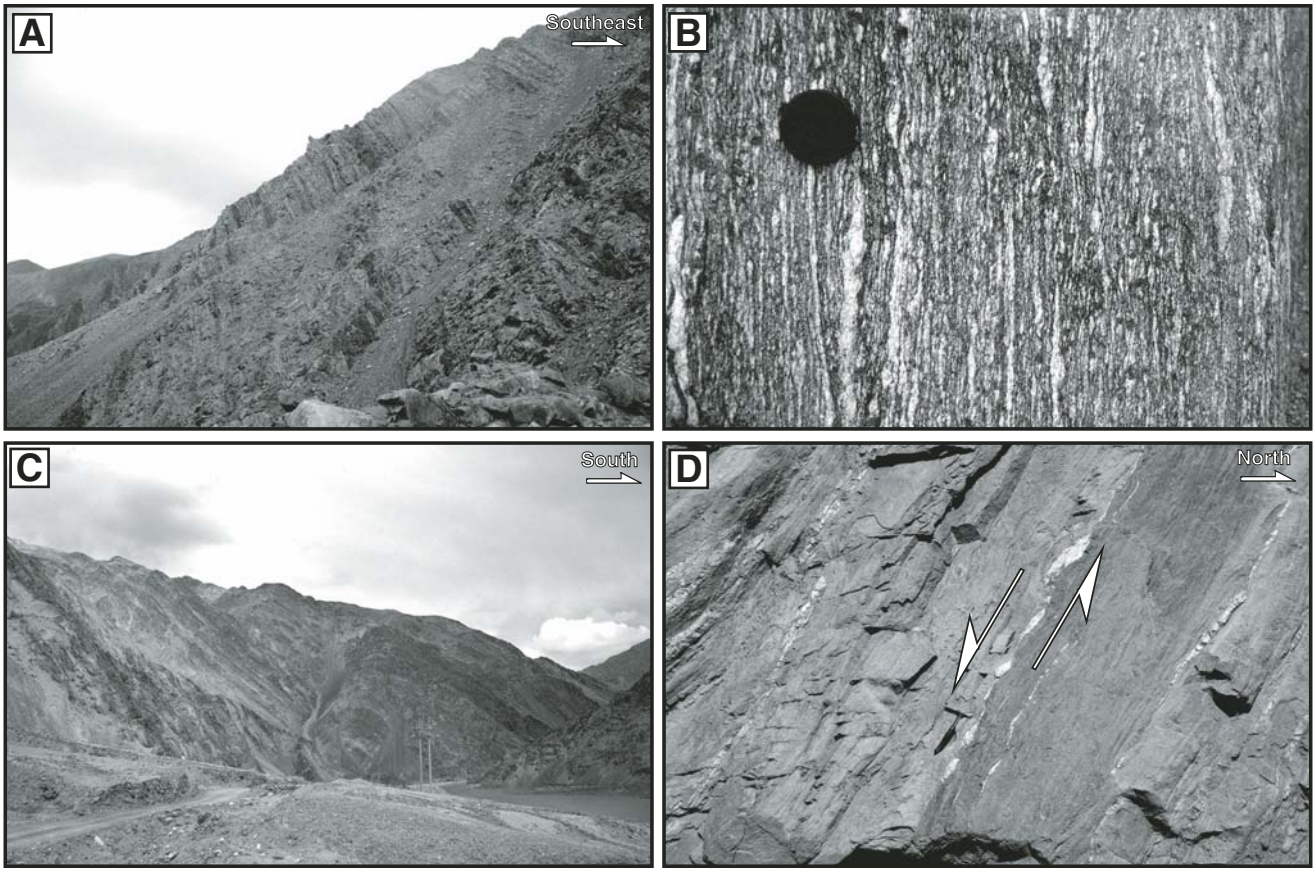

Figure 7. Gneisses of (A) Pz_{gn1} showing typical layering between the quartzofeldspathic gneisses and biotite-hornblende–rich gneisses in the core of the Muztaghata massif. (B) Pz_{sch3} showing migmatitic textures in the high-grade pelitic schists. Lens cap for scale. (C) Looking east at south-dipping Pz_{sch3} at the southern tip of the Kongur Shan normal fault along the Tashkorgan River. (D) Looking west at Pz_{sch3} immediately north of the Shen-ti fault. Asymmetric boudinage of a quartz vein shows top-south sense of shear. Rock hammer for scale. Qtz—quartz; Chl—chlorite; Act—actinolite; Plg—plagioclase; Ky—kyanite; Grt—garnet.

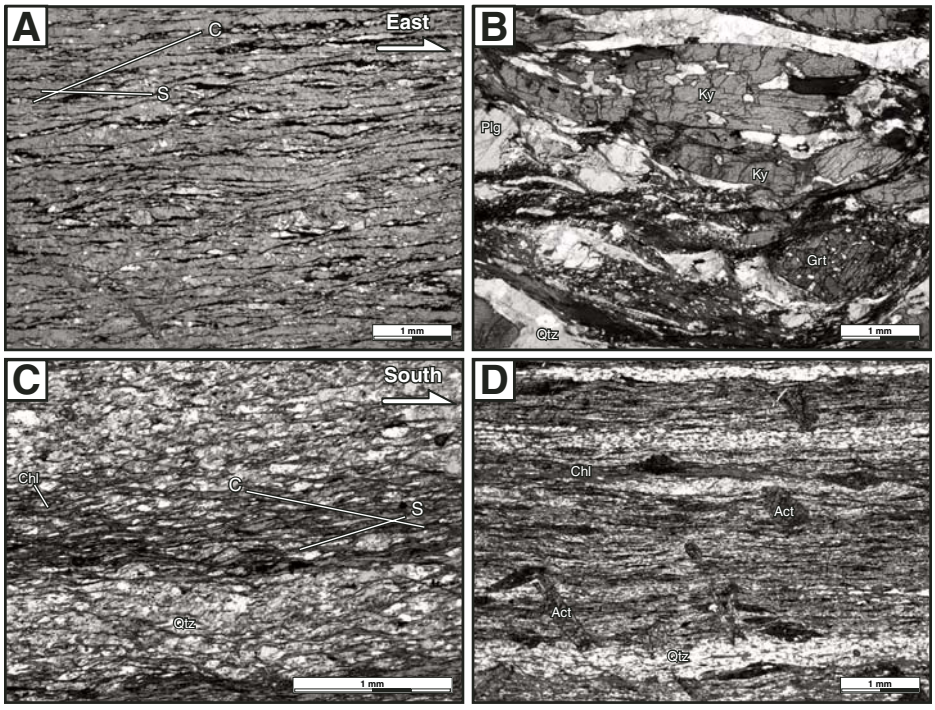

Figure 8. Photomicrographs of metamorphic units along the southern Kongur Shan extensional system. (A) Mylonitic schist of Pz_{sch3} from the western flank of Muztaghata with top-to-the-west sense of shear. Outcrop is ~200 m high. (B) Garnet-kyanite-K-feldspar assemblage of Pz_{sch3} from sample AR7/7/00-7a. (C) Mylonitic S-C fabric in quartz-rich schist from Pz_{sch4} showing top-to-the-south sense of shear. Relief is ~800 m. (D) Mafic schist from Pz_{sch4} with actinolite crosscutting foliation.

schists and quartzofeldspathic gneisses from the footwall of the Kongur Shan normal fault are juxtaposed against structurally higher medium-grade schists of Pz_{sch4} (Figs. 3 and 5). Pz_{sch4} is composed of interlayered quartz-rich, calcareous, and mafic schists. Mafic schists consist of chlorite + quartz + epidote ± actinolite ± calcite (Figs. 8C and 8D), indicating greenschist facies metamorphic conditions. Actinolite porphyroblasts crosscut the foliation in several samples, suggesting postdeformation peak metamorphic conditions (Fig. 8D). Pz_{sch4} continues to the southeast, where it is exposed along the eastern side of the Wuqa Valley (Figs. 3 and 4).

Structurally above the greenschist facies schists of Pz_{sch4} and exposed between the Tashkorgan Valley and Wuqa Valley are high-grade schists of Pz_{sch5} (Figs. 5–6). Pz_{sch5} consists of pelitic schists and quartzofeldspathic gneisses intruded by small bodies of undeformed to mylonitic granite. Metamorphic grade in the unit decreases to the south from upper amphibolite facies (garnet ± sillimanite ± kyanite ± K-feldspar) to greenschist (garnet + biotite) facies.

STRUCTURAL GEOLOGY OF THE SOUTHERN KONGUR SHAN

Kongur Shan Extensional System

From north to south, the 250-km-long Kongur Shan extensional system consists of the Muji fault, Kongur Shan normal fault, Tahman normal fault, and Tashkorgan normal fault (Figs. 2 and 3) (Robinson et al., 2004). The geology of the northern portion of the extensional system including the Muji fault and the northern segment of the Kongur normal fault has been previously described by Arnaud et al. (1993), Brunel et al. (1994), and Robinson et al. (2004). Here, we describe the structures along the central and southern segments of the Kongur Shan extensional system. Together with previously published work, our new results provide a coherent view of the overall structural framework of the Kongur Shan extensional system.

Southern Kongur Shan Normal Fault

The Kongur Shan normal fault is generally north-striking south of the Kongur Shan massif, but it becomes highly convex to the west along the western margin of the Muztaghata massif (Figs. 3 and 5). While the location of the fault is easy to determine in the field within a few meters and by satellite images, the fault trace itself is commonly buried under glacial deposits and other Quaternary debris and was not directly observed. Along the western flank of the Muztaghata massif, a 5–10-m-thick zone of chloritic breccia is present, immediately beneath which are mylonitic schists and high-grade gneisses with west-plunging stretching mineral lineations. Kinematic indicators such as S-C fabrics and rotated quartz pods show top-to-the-west sense of shear (Figs. 7A). Mylonitic fabrics die out ~200 m below the fault surface at deeper structural levels and are also absent along the southern flank of Muztaghata. Foliations in the schists and gneisses and compositional banding in the gneisses are generally parallel to the slope of the western mountain flank of the Muztaghata massif, dipping ~30° west and increasing to ~60° southwest along the southern flank of the massif (Figs. 5, 6A, and 6B). The 30° dip of the mylonitic foliations along the western Muztaghata flank is interpreted to be subparallel to the dip of the Kongur Shan normal fault.

Foliations within the Muztaghata massif define a west-northwest–trending antiform, with a gently dipping northern limb and a moderately dipping southern limb (Figs. 5 and 6D). Field observations in the eastern core of the massif indicate the foliation rotates to the east from west-dipping to subhorizontal (Figs. 6A and 6B). This is notably different from the structure of the Kongur Shan gneiss dome to the north (Brunel et al., 1994; Robinson et al., 2004), where foliations define a north-northwest–trending, north-plunging dome, with the axis subparallel to the strike of the Kongur Shan normal fault and steeply (>70°) east-dipping foliations along the eastern limb of the dome.

The Kongur Shan normal fault continues for ~20 km south of the Tagamansu Valley before terminating at the Tashkorgan River (Fig. 5). Along this segment of the fault, the internal structure of the footwall changes significantly: Footwall foliations and compositional layering change from orientations subparallel to the strike of the Kongur Shan fault to highly oblique. At the southern tip of the Kongur Shan fault, foliations are perpendicular to the fault, striking east-west and dipping moderately to the south (Figs. 5 and 7C). Mylonitic fabrics and stretching lineations are abundant in the southern exposures of Pz_{sch3}, with generally south-plunging orientations and top-to-the-south sense of shear (Fig. 7D). The contact between footwall units Pz_{gn} and Pz_{sch3} is cut at a high angle by the Kongur Shan normal fault and continues across the fault into the footwall of the Tahman normal fault with little or no observable offset (Fig. 5). This is the only place along the trace of the Kongur Shan normal fault where rock units can be mapped across the structure, supporting the observation that the fault terminates in this area.

Tahman Normal Fault

The 20-km-long Tahman normal fault cuts obliquely across the northern end of the Tashkorgan Valley, strikes N25°E along the northern two-thirds of the fault and N5°E along the southern third of the fault, and dips steeply to the west-northwest (Fig. 5). Quaternary activity along the fault is demonstrated by well-preserved 1–2-m-high fault scarps that cut Quaternary alluvial deposits. Maximum local relief in the footwall of ~500 m suggests low magnitudes of offset across the fault. The Tahman fault is interpreted to be a transfer structure, linking the west-dipping Kongur Shan normal fault and the east-dipping Tashkorgan normal fault. As with the southern end of the Kongur Shan normal fault, footwall structures and fabrics in the high-grade schists and gneisses are truncated at a high angle by the Tahman fault and show no relation to the active structure. Mineral lineations and shear sense indicators in the metamorphic rocks trend generally north-south and are top-to-the-south, respectively.

Muztaghata Dome

North-south cross sections through the footwall of the Kongur Shan and the Tahman normal faults (Figs. 8C and 8D) show that the high-grade schists and gneisses of Pz_{sch3} and Pz_{gn1} define a large upright to slightly overturned south-vergent antiform with the west-plunging domal structure of the Muztaghata massif described above as defining the hinge of the structure. Since the active Kongur Shan and Tahman normal faults clearly crosscut the southern limb of this antiform, the domal structure of the Muztaghata massif is interpreted to largely predate the initiation of east-west extension along the Kongur Shan extensional system.

Tashkorgan Normal Fault

The 75-km-long Tashkorgan normal fault is the southernmost segment of the Kongur Shan extensional system. The fault strikes north to north-northwest, dips steeply to the east, and bounds the western side of the Tashkorgan Valley (Figs. 3 and 4). Expression of the fault is variable along strike: North of the junction with the Tahman normal fault along the gently sloping western side of the valley, interpretation of satellite images shows that the Tashkorgan normal fault consists of several discontinuous faults 5–10 km in length (Fig. 3). South of the juncture with the Tahman fault, the Tashkorgan normal fault becomes a prominent morphologic feature, bounding the western side of the valley (Figs. 3 and 4), with well-developed triangular facets along the eastern flank of the mountain range. The Tashkorgan fault is well defined for another 30 km to the south, while topographic relief of the footwall decreases. At its southern tip, the fault branches into two smaller faults, which form scarps with ~100 m of offset within

a loess-covered region (Q_l) on the western side of the Tashkorgan Valley (Fig. 4). Offset of the loess dies out to the south over a distance of ~10 km, and the Tashkorgan fault is interpreted to terminate without linking to structures further south. An $^{40}Ar/^{39}Ar$ K-feldspar cooling age from the syenite in the northern footwall of the Tashkorgan normal fault of 54 Ma (Xu et al., 1996) indicates temperatures below 150 °C since the early Eocene, indicating ≤5 km of exhumation due to late Cenozoic east-west extension (assuming a geothermal gradient of 30 °C/km).

Kalaqigu Fault

Directly along strike south of the southern termination of the Tashkorgan fault, a north-south–striking subvertical gouge zone, 40–50 m thick, called the Kalaqigu fault, separates beige to gray Jurassic marbles to the west from Permian slates to the east (Fig. 4). No clear kinematic indicators were found within the gouge zone, and no offset features were identified to determine a sense of shear. While the Kalaqigu fault is in the correct orientation to link the active Kongur Shan extensional system to the north and the Karakorum fault to the south, as has been previously proposed (Arnaud et al., 1993; Brunel et al., 1994; Ratschbacher et al., 1994; Strecker et al., 1995; Murphy et al., 2000), our field observations indicate that the fault has not been recently active (Figs. 4A and 4D). Specifically, the fault trace cuts perpendicularly across several narrow, deeply incised valleys without offsetting them, and ridges above the valleys where the gouge zone is exposed are capped by Quaternary loess deposits that show no evidence of tectonic disturbance.

Shen-ti Normal Fault

At the southern tip of the Kongur Shan normal fault, upper amphibolite facies schists and gneisses in the footwall of the Kongur Shan and Tashkorgan faults (Pz_{sch3} and Pz_{gn}) are separated from greenschist facies schists to the south (Pz_{sch4}) along the east-west–trending Shen-ti fault (Fig. 5). The Shen-ti fault cuts obliquely through the high-grade schists and gneisses in its footwall juxtaposing the low-grade Pz_{sch4} against high-grade pelitic schists (Pz_{sch3}) to the west and quartzofeldspathic gneisses (Pz_{gn}) to the east. While exposures of fault gouge were observed along the trace of the fault, the fault surface that bounds the hanging wall and the gouge zone was never directly observed in the field. Subparallel south-dipping foliations in the hanging wall and footwall along most of the trace of the Shen-ti fault are interpreted to indicate a southerly dip, although to the east, footwall fabric orientations within the quartzofeldspathic gneisses are moderately to highly oblique to the orientation of the Shen-ti fault (Fig. 5). Kinematic indicators in the southern exposures of the high-grade schists show top-to-the-south sense of ductile shear adjacent to the Shen-ti fault (Fig. 7D), while mylonitic S-C fabrics within the calcareous and mafic schists in the hanging wall of the Shen-ti fault also show top-to-the-south sense of shear (Fig. 8C). Top-to-the-south shear sense indicators and the juxtaposition of high-grade rocks in the footwall against lower-grade rocks in the hanging wall all suggest that the Shen-ti fault is a top-to-the-south normal fault. The east-west change in footwall units and fabric orientations suggests that the brittle Shen-ti fault cuts obliquely through the footwall, exposing structurally deeper (and non-mylonitic) portions of the footwall to the east (Fig. 5).

Torbashi Thrust

Immediately south of the Shen-ti fault, greenschist facies calcareous and mafic schists of Pz_{sch4} are juxtaposed against upper amphibolite facies schists of Pz_{sch5}, indicating the presence of a fault we call the Torbashi fault (Figs. 3–4). The contact between Pz_{sch4} and Pz_{sch5} is strikes east subparallel to the Shen-ti fault before bending to the southeast along the Wuqa Valley (Fig. 4). Foliations in the low-grade footwall schists and high-grade hanging-wall schists generally follow the orientation of the contact, changing from east-striking and south-dipping along the Tashkorgan River to northwest-striking, southwest-dipping along the Wuqa Valley. Although we never directly observed the Torbashi fault in the field, south- to southwest-dipping foliations on either side of the inferred fault trace imply a south- to southwest-dipping fault, with mylonitic fabrics in the hanging wall showing top-to-the-southwest shear sense (Fig. 4). Based on the juxtaposition of high-grade schists structurally overlying low-grade schists, we interpret the Torbashi fault to be an originally northwest-dipping, southwest-directed thrust, which has been subsequently rotated to a southerly dip. Along the eastern side of the Tashkorgan Valley, fabrics in the high-grade schists in the hanging wall of the Torbashi thrust change to the south from south-southwest–dipping to northeast-dipping, with east-west– to southwest-northeast–trending mineral lineations (Fig. 4). Further south, northeast-dipping medium-grade schists (Pz_{sch5}) lie structurally above northeast-dipping Permian limestones and slates. As to the north, the juxtaposition of higher-grade rocks over lower-grade rocks suggests that the contact is a thrust fault that dips to the northeast. We interpret this contact to be the southern exposure of the Torbashi thrust, where the high-grade rocks of Pz_{sch5} form a large synformal klippe.

GEOCHRONOLOGY AND THERMOCHRONOLOGY

In order to better understand the tectonic evolution of the southern Kongur Shan region, we used several techniques to determine the timing of igneous activity, high-grade metamorphism, and exhumation of the various units. These included U-Pb isotopic analyses of individual zircon grains and in situ Th-Pb isotopic analyses of individual monazite grains using the UCLA CAMECA IMS 1270 ion microprobe, and $^{40}Ar/^{39}Ar$ step-heating analyses of biotite and muscovite separates from numerous samples. Analytical procedures for the various techniques are the same as those described in Robinson et al. (2004) and references therein.

U-Pb Zircon Geochronology

Cenozoic Biotite Granite

Twenty-seven zircon grains from three samples (AY8/21/99–8, AY8/23/99–3, and AR4/27/00–10) were analyzed from the large biotite granite in the hanging wall of the Kongur Shan normal fault west of the Muztaghata massif (M_{gr}; Fig. 5; Table DR3 [see footnote 2]). Zircon analyses yielded a spread in ages from Late Proterozoic to late Miocene, with a strong cluster of late Miocene ages (Figs. 9A and B). Older ages generally came from the cores of zircon grains and are interpreted as inherited zircon from the protolith. The seventeen youngest analyses from the biotite granite yielded a weighted mean $^{206}Pb/^{238}U$ age of 11.46 ± 0.71 Ma (mean square of weighted deviates [MSWD] = 5.5), while a strong cluster of 12 analyses yielded an indistinguishable age of 11.68 ± 0.45 (MSWD = 1.5) (Fig. 9B), which we interpret as the intrusion age of the granite.

Footwall Orthogneiss

Sample AR6/15/00–3 was collected from a deformed biotite granite located in the footwall of the Kongur Shan normal fault immediately north of the Muztaghata massif (Fig. 5). Fourteen analyses were made from 11 zircon grains (Fig. 9C). One analysis (11–2) yielded a negative U-Pb $^{206}Pb^*/^{238}U$ age with large errors and is not discussed further. The other analyses yielded Late Cretaceous to early Miocene $^{206}Pb^*/^{238}U$ ages (105–22 Ma), with nine analyses yielding late Eocene to early Miocene $^{206}Pb^*/^{238}U$ ages of 22–44 Ma. The nine youngest ^{204}Pb corrected ages were slightly reversely discordant, and two analyses yielded negative $^{207}Pb^*/^{235}U$ ages (analyses 8–1 and 1–1; Table DR3).

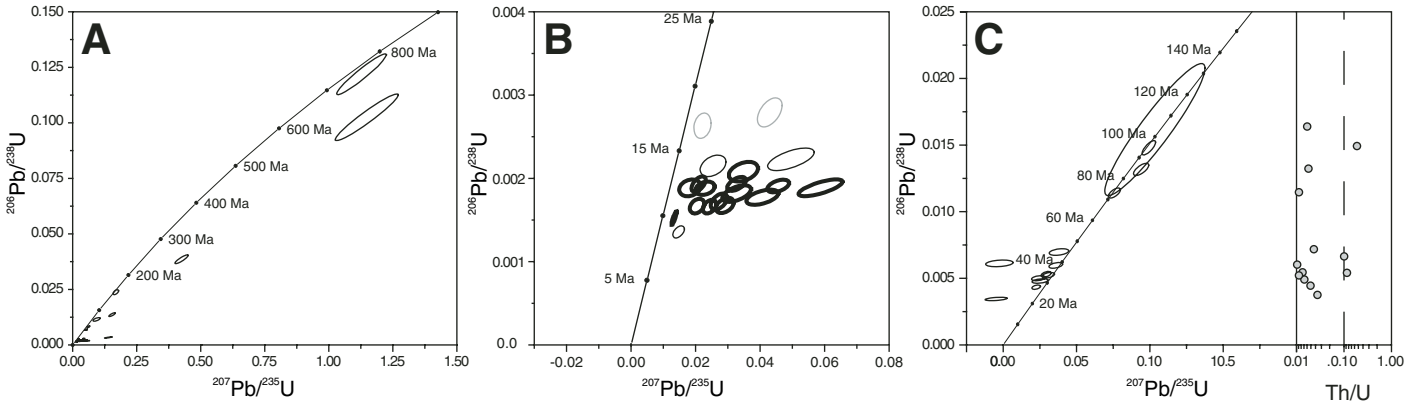

Figure 9. Concordia plots of U-Pb zircon analyses. (A) All zircon analyses from biotite granite M_{gr} (samples AR4/27/00–10, AY8/21/99–8, and AY8/23/99–3). (B) Miocene analyses from biotite granite M_{gr}. Analyses in black yield a weighted mean age of 11.46 ± 0.71 Ma (mean square of weighted deviates [MSWD] = 5.5). Analyses in bold yield a weighted mean age of 11.68 ± 0.45 Ma (MSWD = 1.5). (C) Zircon analyses from footwall mylonitic granite (sample AR 6/15/00–3). The Th/U ratios for each analysis are plotted to the right of the concordia plot.

Zircon grains from AR6/15/00–3 have a mottled internal zoning pattern in cathodoluminescence images, and several grains contain small patches of truncated oscillatory zoning (Fig. DR4, see footnote 2). Analyses show a direct correlation of age with internal zoning: Spot analyses of overlapping portions of oscillatory zoned zircon yield Late Cretaceous ages while analyses exclusively from mottled portions of zircon yield Cenozoic ages. The mottled internal zoning is interpreted to be zircon grown or recrystallized during high-grade metamorphism (Hoskin and Black, 2000), while oscillatory zoned patches represent preserved portions of premetamorphic igneous zircon. This interpretation is supported by low Th/U ratios of the analyses (Th/U < 0.10; Fig. 9C) typical of metamorphic zircon (e.g., Hoskin and Black, 2000; Ding et al., 2001; Mojzsis and Harrison, 2002). The timing of metamorphism is tentatively placed as Oligocene–early Miocene based on the six youngest analyses (33–22 Ma).

Th-Pb Monazite Geochronology

Seven samples from the high-grade pelitic schists of Pz_{sch3} were dated by in situ ion-microprobe Th-Pb analyses of monazite from two different regions: the western flank of Muztaghata, and the southern footwall of the Kongur Shan and footwall of the Tahman fault (Fig. 5) (Table DR4, see footnote 2).

Thirty-five grains were analyzed from three samples of mylonitic high-grade schist from the western flank of Muztaghata (AR 8/31/03–3, AR 8/31/03–5, and AR 9/1/03–1a) (Fig. 5), seven of which occurred as inclusions in garnet and twenty-eight of which were from the matrix of the sample. Analyses of monazite inclusions in garnet yielded ages from Triassic (228 ± 10 Ma) to late Oligocene (24.1 ± 1.7 Ma). Matrix analyses all yielded Miocene ages from 15.9 ± 0.3 Ma to 7.5 ± 0.2 Ma. Sixty-eight monazite grains were analyzed from four samples of garnet–kyanite–K-feldspar–bearing rocks at the southern end of the Kongur Shan normal fault footwall and the footwall of the Tahman normal fault (AR 9/6/03–3, AR 9/6/03–5, AR 7/7/00–7a, and AR 7/8/00–5b) (Fig. 5); thirty-seven of these occurred as inclusions in garnet, and thirty-one were from the matrix of the sample. Analyses from monazite inclusions in garnet (almost entirely from samples AR 7/7/00/7a and AR 7/8/00–5b) yielded ages from Jurassic to middle Miocene. With one exception, matrix monazite analyses yielded Oligocene to Miocene ages, with most falling between 10 and 16 Ma.

The cumulative distribution of all analyses from monazite inclusions in garnet from Pz_{sch3} yielded a wide spread in ages from Mesozoic to Miocene (Fig. 10). Mesozoic ages ranged from Middle Triassic to Late Cretaceous, and most ages fell between the Middle Jurassic and Early Cretaceous. While the Mesozoic ages indicate a polymetamorphic history for Pz_{sch3}, the wide spread makes it difficult to determine the timing of this earlier metamorphic event (or events). Cenozoic ages from monazite inclusions in garnet ranged from Eocene to middle Miocene with two main peaks: (1) a broad Oligocene to early Miocene peak from 30 to 20 Ma, and (2) a narrow middle Miocene peak at ca. 14 Ma. Matrix monazite analyses yielded only one pre-Oligocene age of 119.2 ± 5.7 Ma (Fig. 10). The cumulative distribution of Cenozoic matrix ages show three main peaks: (1) a small broad late Oligocene to early Miocene peak (ca. 20–25 Ma), which overlaps with the first peak in inclusion ages, (2) a narrow middle Miocene peak at ca. 14 Ma, which overlaps with the second peak in inclusion ages, and (3) a broad peak in the late Miocene from ca. 11 to 8 Ma that is not present in the distribution of garnet inclusion ages.

Based on the distribution of the inclusion and matrix ages, together with the high grade of metamorphism and migmatitic textures, we interpret the monazite analyses as follows: Cenozoic burial and prograde metamorphism of the schists and gneisses to mid-crustal depths (30–35 km based on thermobarometry) occurred during the Oligocene–early Miocene, resulting in the broad peak in ages in both the matrix and inclusion analyses (as well as the metamorphic zircon ages from AR6/15/00–3). Continued crustal thickening and/or thermal relaxation during the Miocene led to partial melting of the schists at ca. 14 Ma, resulting in the narrow peak in ages in

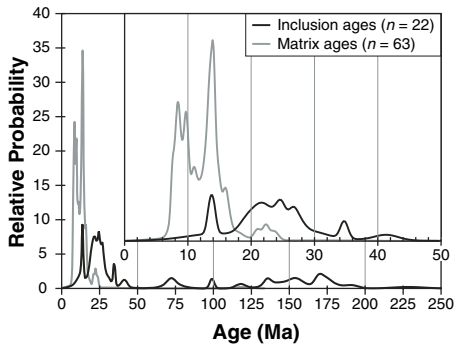

Figure 10. Cumulative probability plots of all monazite Th-Pb ages from Pz_{sch3} grouped into inclusion ages (black) and matrix ages (gray).

both matrix and inclusion analyses. Since monazite in the matrix of the samples would have been susceptible to dissolution/reprecipitation during anatexis, much of the monazite grown during the Oligocene–early Miocene (as well as surviving Mesozoic grains) would have been reset or destroyed. Recrystallization processes during exhumation-related deformation resulted in continued monazite growth, producing late Miocene matrix ages from 8 to 10 Ma.

$^{40}Ar/^{39}Ar$ Thermochronology

Hanging Wall of Kongur Shan Normal Fault

A sample from Pz_{sch1} in the hanging wall of the Kongur Shan normal fault (AR6/19/00–11a) northwest of the Muztaghata massif (Fig. 3) yielded a Late Jurassic biotite age of 159 ± 4 Ma (Table DR5, Fig. DR5, see footnote 2), which overlaps with previously published Late Jurassic ages from the northern portion of the hanging wall (Robinson et al., 2004). As discussed in Robinson et al. (2004), we interpret these ages to reflect postmetamorphic cooling through the biotite closure temperature.

Sample AR4/27/00–10 is from the biotite granite at the northern end of the Tashkorgan alkaline complex (M_{gr}), southwest of the Muztaghata massif (Fig. 5). This sample yielded a biotite $^{40}Ar/^{39}Ar$ weighted mean spectra age of 11.2 ± 0.2 Ma, which is in agreement with the biotite and K-feldspar cooling ages from Xu et al. (1996) and overlaps the U-Pb zircon age of 11.68 ± 0.45 Ma. The overlap in age between the zircon U-Pb analyses and the biotite and K-feldspar $^{40}Ar/^{39}Ar$ analyses shows that the granite was emplaced at shallow depths and cooled rapidly in the middle Miocene.

Footwall of Kongur Shan Normal Fault

Twenty-two biotite analyses and five muscovite analyses were obtained from samples taken from the footwall of the Kongur Shan normal fault (Fig. 4). Most analyses yielded relatively flat age spectra with agreement within error between total gas, weighted mean age spectra, and inverse isochron ages. Several analyses yielded slightly disturbed, but interpretable age spectra (e.g., AR7/4/00-1; Fig. DR5Z), while one analysis yielded a highly disturbed uninterpretable age spectra (AR6/30/00-10b; Fig. DR5W).

North of the Muztaghata massif, muscovite and biotite analyses from footwall gneisses yielded ages of 6.2–2.7 Ma (Fig. 5). The data from this area show two trends: (1) ages increase slightly to the east with distance from the fault, and (2) ages increase to the south along the trace of the fault, where muscovite ages increase from 2.9 Ma to 6.2 Ma over a distance of 10.5 km along the northern flank of Muztaghata.

South of the Muztaghata massif, biotite and muscovite analyses from the footwall of the Kongur Shan normal fault are characterized by remarkably consistent ages of 7.5–8.5 Ma over a broad area (Fig. 5). One biotite age of 10.1 ± 0.2 Ma at the mouth of Tugenmansu Valley is anomalously old, which we interpret to be due to excess ^{40}Ar. While there was only one muscovite analysis along the southern footwall of the Kongur Shan normal fault (AR7/4/00–5), the age overlaps with nearby biotite ages, indicating rapid cooling in the late Miocene. These ages are in general agreement with two phlogopite K-Ar ages and a biotite K-Ar age reported by Xu et al. (1996) of 9.0 Ma, 6.7 Ma, and 6.7 Ma, respectively, from the Tugenmansu Valley. However, since no uncertainties were reported, it is difficult to assess the discrepancy of their younger ages. The consistency of the ages from the footwall is notable because there are no obvious relationships between the biotite ages and proximity to the Kongur Shan fault, structural trends, or rock type. This is strikingly different from the pattern of increasing age with distance from the Kongur Shan fault observed in the footwall immediately north of the Muztaghata massif and along the northern flank of the Kongur Shan massif (Arnaud et al., 1993; Robinson et al., 2004).

Footwall of Tahman Normal Fault

Four biotite and two muscovite analyses were obtained from schists of Pz_{sch3} within the footwall of the Tahman fault (Fig. 5). Analyses from the Tahman fault footwall generally yielded ages of 8–10 Ma, which overlap with footwall ages from the Kongur Shan fault directly to the east. One analyses from the footwall of the Tahman normal fault yielded a biotite age of 13.7 Ma, which we interpret to be the result of excess ^{40}Ar because it overlaps with the timing of peak metamorphic conditions for the footwall determined from monazite Th-Pb geochronology.

Hanging Wall of Torbashi Fault

Three biotite analyses and one muscovite analysis were obtained from high-grade schists of Pz_{sch5} at the northern end of the Torbashi fault hanging wall (Fig. 5; Figs. DR5AJ–DR5AM [see footnote 2]). Biotite analyses yielded late Early Cretaceous total gas ages between 107 ± 2 Ma and 124 ± 4 Ma, with somewhat disturbed age spectra. The muscovite analysis yielded an erratic age spectra with a total gas age of 105 Ma. Since this is significantly younger than the biotite age of 120 Ma from the same sample, it suggests that either the biotite is contaminated with excess ^{40}Ar, or the muscovite has been subjected to alteration. Despite the relatively poor quality of the data, these results indicate that the high-grade schists in the hanging wall of the Torbashi thrust fault were cooled below the muscovite and biotite closure temperatures by the Late Cretaceous.

DISCUSSION

Field investigations of the southern Kongur Shan extensional system and related geochronologic and thermochronologic analyses provide insight into the Cenozoic tectonic evolution and pre-Cenozoic tectonic configuration of the Pamir region. Next, we discuss the geologic implications of our observations and analytical results.

Kongur Shan Extensional System

Cooling-age patterns and geologic relations across the active faults at the southern end of the Kongur Shan extensional system provide important information on the magnitude and timing of extension along the southern end of the Kongur Shan extensional system. While cooling ages in the footwall of the southern Kongur Shan fault and Tahman fault are uniformly late Miocene, several observations demonstrate that this cooling event was unrelated to the active east-west extension: (1) late Miocene cooling ages show no variation relative to the active structures, with little or no offset in ages across the Kongur Shan fault and no variation in cooling ages up to at least 15 km east of the active Kongur Shan fault (Fig. 5). (2) Kinematic indicators in the southern exposures of Pz_{sch3}, which were at ~35 km in the middle Miocene show top-to-the-south sense of shear, perpendicular to the active east-west extension. (3) The sharp break in cooling ages from Miocene to Cretaceous and between upper amphibolite and greenschist facies schists occurs across the south-dipping Shen-ti fault. (4) Geologic mapping shows no detectable offset of the contact between the high-grade schists (Pz_{sch3}) and quartzofeldspathic gneisses (Pz_{gn1}) across the Kongur Shan fault and no observable continuation of the fault south of the Tashkorgan River.

Cooling ages along the northern flank of the Muztaghata massif are more difficult to uniquely interpret. The decrease in cooling ages across the massif from ca. 7.5 Ma to 6.2 Ma and younger could represent a break between pre–east-west extension ages to the south and syn-extensional ages to the north. This would date initiation of extension along the southern end of the Kongur Shan fault to between 6.2 and.5 Ma, similar to the documented initiation of extension at the northern end of the fault (Robinson et al., 2004). Alternatively, the 6.5 Ma muscovite age could represent cooling due to re-equilibration of high thermal gradients from rapid middle to late Miocene exhumation of the schists and gneisses immediately to the south. If so, ages

farther north would suggest initiation of extension since ca. 5 Ma, indicating southward propagation of east-west extension.

Regardless of these two interpretations, cooling ages indicate that the southernmost change from pre– to syn–east-west extension ages occurs along the western flank of the Muztaghata massif, where we interpreted the fault to dip ~30° to the west. Rapid middle to late Miocene exhumation documented immediately to the south would have resulted in advection of isotherms and a high local geothermal gradient along the Muztaghata massif. Using a reasonable elevated geothermal gradient of 40 °C/km, rocks along the western flank of the massif at or near the biotite and muscovite closure temperatures would record ~9 km of exhumation, yielding ~20 km of east-west extension, with higher geothermal gradients (or synextensional ages located farther north) yielding less extension.

Eocene K-feldspar cooling ages demonstrate <5 km of exhumation along the steeply east-dipping Tashkorgan, which results in <3 km of extension for a fault dipping 60°. This, along with the apparent termination of the fault to the south within thick Quaternary(?) deposits, shows low magnitudes of extension along the Tashkorgan fault and a southward decrease in the magnitude of extension along the southern half of the Kongur Shan extensional system.

To address along-strike variation of east-west extension along the entire Kongur Shan extensional system, it is necessary to reexamine one of our calculations from Robinson et al. (2004). One of the two points where magnitudes of extension were calculated along the Kongur Shan normal fault was ~35 km north of the Kongur Shan massif, where K-feldspar Multiple Diffusion Domain modeling showed rapid cooling from ~250 °C at 7–8 Ma. The segment of the fault where the sample was located dips ~30° to the southwest, and the calculated 17 km of extension was based on ~10 km of exhumation along a 30°-dipping plane. However, since extension is east-west rather than northeast-southwest, exhumation would be along a path plunging ~20° west, yielding ~30 km of east-west extension. While we did not obtain detailed kinematic data in the field, analysis of satellite images indicates right-lateral deflection of geomorphic features along this fault segment, which is consistent with the above interpretation. It is important to note that the estimated magnitude of extension is still less than the ~35 km of extension calculated along the Kongur Shan massif farther to the south.

East-West Extension in the Pamir

Calculated magnitudes of extension along the Kongur Shan fault system from north to south are as follows: (1) ~30 km at the northern end of the Kongur Shan fault, (2) ~35 km along the Kongur Shan massif, (3) ~20 km (or less) along the Muztaghata massif, and (4) <3 km along the Tashkorgan fault. While uncertainties in the individual calculations are significant, due primarily to uncertainties in subsurface fault geometry (e.g., if the fault shallows at depth) and geothermal gradients, the overall pattern of decreasing magnitude of extension from north to south is robust. These results are consistent with east-west extension in the Pamir that was primarily driven by oroclinal bending–radial spreading of the Pamir salient during northward overthrusting along the Main Pamir thrust.

One key observation is that our calculations show the largest magnitude of extension located along the Kongur Shan massif; this is inconsistent with a simple oroclinal bending–radial spreading model, which would predict a constant southward decrease in the magnitude of extension. This suggests that other factors play a role in the evolution of the Kongur Shan extensional system, such as synorogenic uplift associated with the exhumation of the Kongur Shan massif (e.g., Brunel et al., 1994).

Oligocene-Miocene Crustal Thickening and Gneiss Dome Formation

Oligocene-Miocene Crustal Thickening

Monazite and zircon ages from high-grade schists and gneisses along the southern footwall of the Kongur Shan fault document crustal thickening in the eastern Pamir during the Oligocene to middle Miocene. The timing of crustal thickening overlaps with the interpreted late Oligocene initiation of slip along the Main Pamir thrust as determined from sedimentologic, thermochronologic, and paleomagnetic evidence in the Tarim and Tajik Basins (e.g., Thomas et al., 1994, 1996; Sobel and Dumitru, 1997; Burtman, 2000), as well as metamorphic ages from near-ultrahigh-pressure crustal xenoliths from the southeast Pamir (Ducea et al., 2003; Hacker et al., 2005). Together, these studies point to a major change in the dynamics of the Pamir in the late Oligocene with the initiation of major crustal thickening and shortening. Crustal thickening also appears to have led to a period of extensive Miocene middle- and lower-crustal melting based on the presence of migmatitic textures in the high-grade schists, lower-crustal xenoliths that underwent partial melting (Hacker et al., 2005), and numerous Miocene granitic bodies in the Central Pamir (Fig. 11) (Xu et al., 1996; Ducea et al., 2003; Schwab et al., 2004).

Miocene Gneiss Dome Formation

As discussed already, rapid late Miocene exhumation of high-grade schists and gneisses at the southern end of the Kongur Shan normal fault predated the active east-west extension and was instead accommodated in part by the south-dipping Shen-ti fault. Geochronologic and thermobarometric constraints indicate that the schists were brought from 30 to 35 km depth to within 10 km of Earth's surface in ~6 m.y., which requires exhumation rates of 3–4 mm/yr. We interpret this event to have resulted in the formation of the west-northwest–trending domal structure of the Muztaghata massif and southern Kongur Shan fault footwall. Further, several lines of evidence indicate that the Muztaghata antiform is the eastward continuation of the Muskol and Sares antiforms of the Central Pamir (Figs. 2 and 9), and that these features have not been offset from the Qiangtang anticlinorium along the Karakorum fault. These include: (1) Lithologies in the fault-bounded core of Muskol and Sares domes are described as granitic gneisses, kyanite-garnet–bearing micaceous schists, and interlayered marble and amphibolite, with local migmatization of the high-grade schists (Pashkov and Dmitriyev, 1982; Peykre et al., 1982), identical to the high-grade schists and gneisses in the footwall of the Shen-ti fault (Pz_{sch3} and Pz_{gn1}). While there are differences compared to some of the lithologies described by Schwab et al. (2004) (i.e., lack of gabbros and preserved pillow basalts), these appear to be primarily confined to the upper units (and lower metamorphic grades) of their schematic stratigraphic sections. This is consistent with our observation that the Shen-ti fault cuts "down-section" to the east, excising the shallower levels of the domes. (2) Regional geologic maps and interpretation of satellite images show the contact of the southern margin of the Sares antiform intersecting the Tashkorgan Valley ~10 km south of the westward projection of the Shen-ti fault (Figs. 2 and 11) (Pashkov and Dmitriyev, 1982; Yin and Bian, 1992). (3) The axes of the Sares and Muztaghata domes lie directly along strike of each other (Fig. 11) (Pashkov and Dmitriyev, 1982), and restoration of east-west extension places the Muztaghata massif directly beneath the Sares dome. (4) Map relations and interpretation of satellite images suggest that, like the Muztaghata dome, the Sares dome is asymmetric with a shallower-dipping northern limb, defined by a sinuous contact that interacts with local topography, and a steeper-dipping southern limb, which is straighter and does not appear to interact with topography. (5) The Sares and Muskol gneiss domes record early Miocene $^{40}Ar/^{39}Ar$ hornblende and biotite cooling ages, with Cretaceous $^{40}Ar/^{39}Ar$ cooling ages in the Central Pamir south of the domes (101 Ma; Schwab et al., 2004), similar to the age juxtaposition across the Shen-ti and Torbashi faults.

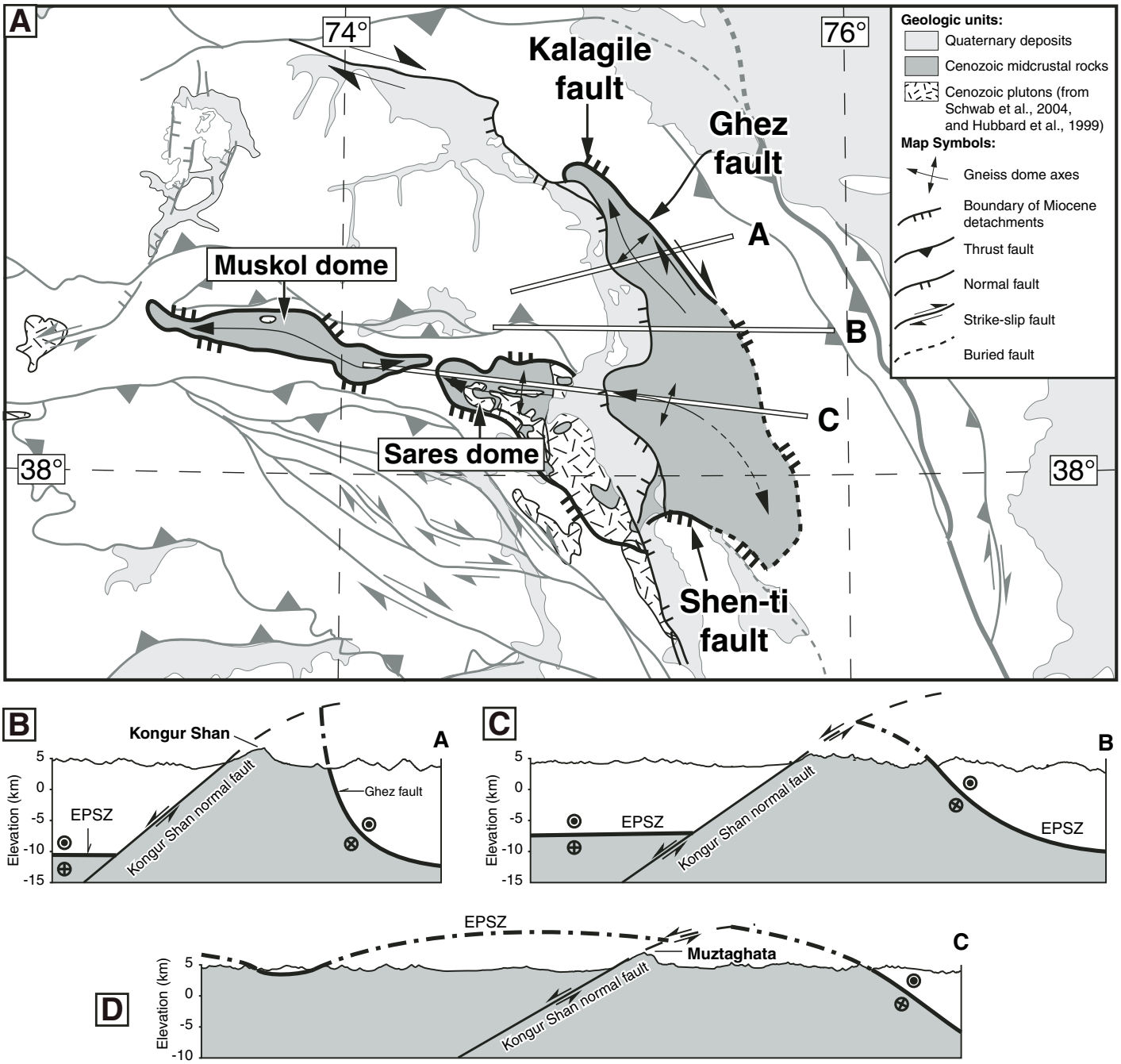

Figure 11. (A) Simplified tectonic map of the Pamir emphasizing Cenozoic high-grade rocks exposed in the cores of the Muskol and Sares domes and the footwall of the Kongur Shan normal fault, and the distribution of the Cenozoic Sares-Murgab belt of plutons in the Pamir. (B–D) Schematic cross sections A, B, and C across the Kongur Shan normal fault and Eastern Pamir shear zone showing the interpreted relation between the two structures. The line denoting the Eastern Pamir shear zone (EPSZ) represents the schematic location of a shear zone several kilometers thick.

Although cooling-age data from Schwab et al. (2004) for the Sares and Muskol domes are limited, they suggest a complicated history of synchronous gneiss dome formation and crustal thickening during the Miocene. Early Miocene cooling ages for the Sares and Muskol domes overlap with prograde metamorphism documented within the Muztaghata gneiss dome and are older than the late Miocene cooling ages in the footwall of the Shen-ti fault. The eastward decrease in cooling ages along the gneiss domes suggests that either gneiss dome formation was diachronous, migrating from east to west, or that exhumation lasted longer in the east than in the west, eventually exhuming rocks that were still undergoing prograde metamorphism in the middle Miocene. We tentatively prefer the latter, based on the apparent eastward increase in north-south width of the Central Pamir gneiss domes (Fig. 11).

Tectonic Model for Crustal Thickening and Gneiss Dome Formation

While the northern margin of the high-grade core of the Sares antiform is fault-bounded, our field observations indicate that the gneisses of the Muztaghata antiform are structurally continuous with those of the Kongur Shan massif to the north, and they form a coherent high-grade metamorphic terrane in the footwall of the Kongur Shan normal fault. This indicates that the tectonic evolution of this metamorphic terrane involved synchronous middle to late Miocene exhumation at its southern end (this study) and continued prograde metamorphism at its northern end (Robinson et al., 2004). Here, we discuss several other regional observations and propose a tectonic model for the evolution of the Cenozoic metamorphic terrane.

One observation from our field studies in the region and previously published information (Burtman and Molnar, 1993) is the lack of Cenozoic internal shortening of the metamorphic rocks that make up the Northern Pamir terrane south of the Oligocene-Holocene fold-and-thrust belt in the Alai Valley. This requires the Miocene crustal thickening and prograde metamorphism documented in the Kongur Shan massif (Robinson et al., 2004) to have been driven by underthrusting of material beneath the Northern Pamir from either the north or the south.

Where the eastern boundary of the Cenozoic high-grade metamorphic terrane has been well documented east of the Kongur Shan massif, it coincides with the right-lateral Ghez shear zone (Fig. 3) (Brunel et al., 1994; Robinson et al., 2004). The $^{40}Ar/^{39}Ar$ cooling ages and thermokinematic modeling from the Kongur Shan massif require significant footwall rollover (>40°) during extension (Robinson et al., 2005), indicating that the right-slip Ghez shear zone has been rotated from an originally shallowly dipping to subhorizontal position (Fig. 11B), with a top-to-the-south sense of shear. While the southward continuation of the eastern boundary of the high-grade metamorphic rocks has not been documented in detail, all regional geologic maps place it in roughly the same location (Figs. 2 and 11A), and several depict it as a fault (e.g., Yin and Bian, 1992; Xinjiang Bureau of Geology and Mineral Resources, 1993). Furthermore, this eastern contact of the terrane is depicted as connecting with the east-striking Shen-ti fault in the south.

We propose that the eastern contact of the Cenozoic high-grade terrane is a continuous shear zone that links with the Shen-ti fault to the south, which we refer to as the Eastern Pamir shear zone (Fig. 11). In our model, the Eastern Pamir shear zone is a regional ductile décollement that accommodated northward relative displacement of the middle and lower crust relative to the upper crust beneath the northeastern Pamir, which allowed Oligocene to Miocene crustal thickening to occur with limited or no shortening in the upper crust of the Northern Pamir (Fig. 12A). Based on metamorphic assemblages within the Ghez shear zone (garnet + biotite) and pervasive ductile shear distributed over a zone several kilometers wide, the Eastern Pamir shear zone was located below the brittle-ductile transition at mid-crustal depths of ~15 km. This is similar to the depth to detachment for low-angle normal fault systems (e.g., Davis and Lister, 1988; Wernicke and Axen, 1988; Lister and Davis, 1989), including those in Tibet (e.g., Kapp et al., 2005). Crustal thickening in the footwall of the ductile décollement led to melting of the middle and lower crust beneath the Central Pamir during the Miocene (Fig. 12B) and the formation of the Sares-Murgab granitoid belt (Fig. 11A). Continued north-south shortening in the footwall of the Eastern Pamir shear zone, facilitated by a decrease in

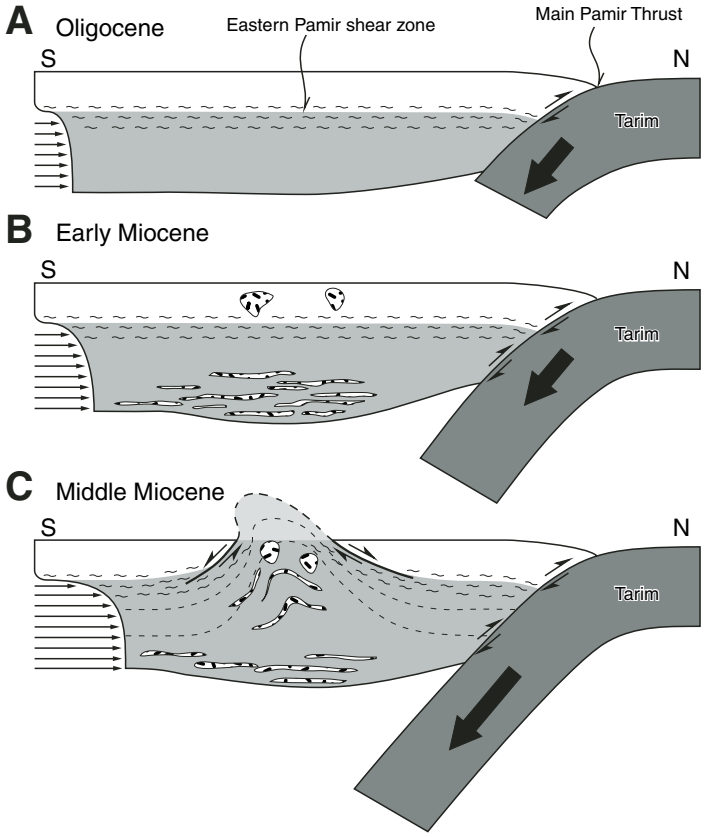

Figure 12. Cenozoic tectonic evolution of the middle and lower crust in the Pamir: (A) Oligocene underthrusting of the middle and lower crust along the Eastern Pamir shear zone with crustal thickening and prograde metamorphism. (B) Continued thickening and heating of the middle and lower crust leads to dehydration melting in the early to middle Miocene, generating granitic melts. (C) Weakened middle and lower crust is extruded upward during continued north-south compression, forming the Central Pamir gneiss domes.

both the density and strength of the footwall of the shear zone due to melting, resulted in extrusion of the Central Pamir gneiss domes synchronous with continued crustal thickening and metamorphism (Fig. 12C) (e.g., Teyssier and Whitney, 2002; Burg et al., 2004; Mahéo et al., 2004). Synchronous gneiss dome formation and continued northward relative motion of the footwall of the Eastern Pamir shear zone during gneiss dome formation accounts for both late Miocene (ca. 9 Ma) prograde metamorphism along the Kongur Shan massif (Robinson et al., 2004) and the asymmetric, south-vergent shape of the Muztaghata gneiss dome (e.g., Whitney et al., 2004).

A possible mechanical drive for our model of deformation, crustal thickening, and gneiss dome formation is the proposed Cenozoic northward subduction of the Karakorum terrane beneath the Central Pamir (Ducea et al., 2003; Hacker et al., 2005). Thus, structures accommodating top-to-the-south Oligocene-Miocene displacement along the Eastern Pamir shear zone footwall would surface where intercontinental subduction was being accommodated, in the southern Karakorum terrane (Fraser et al., 2001), or along one of the suture zones in the Southern Pamir and farther south (Hacker et al., 2005).

CONCLUSIONS

Field and analytical investigations along the southern end of the Kongur Shan normal fault integrated with previously published results from the northern end of the fault system show a generally southward decrease in the magnitude of east-west extension along the Kongur Shan extensional system. These results are consistent with oroclinal bending–radial thrusting of the Pamir salient as the primary driver of east-west extension in the Pamir. However, other processes, such as synorogenic extension, may have played a role in the exhumation of the Kongur Shan massif.

High-grade schists at the southern end of the Kongur Shan extensional system along the Muztaghata massif record upper amphibolite facies metamorphic conditions (~9 kbar, 750 °C), which locally resulted in muscovite dehydration melting. Ion-microprobe Th-Pb monazite and U-Pb zircon ages yield a distribution of ages from the Oligocene to late Miocene, which we interpret to document prograde metamorphism during the late Oligocene to middle Miocene, culminating in partial melting in the middle Miocene. Our interpreted timing of anatexis overlaps with the age distribution of Miocene granitic plutons in the Central Pamir, indicating widespread melting of the middle and lower crust at this time.

Exhumation of high-grade schists and gneisses along the southern Kongur Shan normal fault occurred during the late Miocene prior to initiation of east-west extension, and exhumation of the southern end of the metamorphic terrane was accommodated along the south-dipping, top-to-the-south Shen-ti fault. We interpret this rapid exhumation event, and formation of the Muztaghata antiform, to be related to the development of the Miocene Central Pamir gneiss domes, where the Muztaghata antiform is the eastward continuation of the Sares antiform of Schwab et al. (2004).

Our interpreted eastward continuation of the Sares antiform into the footwall of the Kongur Shan normal fault, and lack of evidence for strike-slip deformation along the Tashkorgan Valley, suggests that the Central Pamir antiforms have not been offset across the Karakorum fault from the Qiangtang anticlinorium as suggested by Schwab et al. (2004).

ACKNOWLEDGMENTS

Discussions with Eric Cowgill, Mike Taylor, and Alex Webb helped clarify many of the ideas presented here. We thank Marty Grove for assistance with the Ar analyses, Frank Kyte for assistance with the electron microprobe analyses, and Marty Grove and Axel Schmidt for support with the ion microprobe analyses and interpretation of data. Careful and critical reviews by Michael Edwards, Rasmus Thiede, and especially Lothar Ratschbacher substantially improved the initial manuscript. Cumulative probability plots were generated using Isoplot/Ex v 3.0 (Ludwig, 2003). This work was supported by National Science Foundation grant EAR-0126122 and a Grants-in-Aid of Research from the Geological Society of America. The ion microprobe facility at University of California–Los Angeles (UCLA) is partially supported by a grant from the Instrumentation and Facilities Program, Division of Earth Sciences, National Science Foundation.

REFERENCES CITED

Arnaud, N.O., Brunel, M., Cantagrel, J.M., and Tapponnier, P., 1993, High cooling and denudation rates at Kongur Shan, eastern Pamir (Xinjiang, China) revealed by $^{40}Ar/^{39}Ar$ alkali feldspar thermochronology: Tectonics, v. 12, no. 6, p. 1335–1346.

Blisniuk, P.M., and Strecker, M.R., 1996, Kinematics of Holocene normal faulting in the Northern Pamir: Eos (Transactions, American Geophysical Union), v. 77, no. 46, p. F693.

Bohlen, S.R., and Liotta, J.J., 1986, A barometer for garnet amphibolites and garnet granulites: Journal of Petrology, v. 27, p. 1025–1034.

Brunel, M., Arnaud, N., Tapponnier, P., Pan, Y., and Wang, Y., 1994, Kongur Shan normal fault: Type example of mountain building assisted by extension (Karakoram fault, eastern Pamir): Geology, v. 22, p. 707–710, doi: 10.1130/0091-7613(1994)022<0707:KSNFTE>2.3.CO;2.

Burg, J.-P., Kaus, B.J.P., and Podladchikov, Y.Y., 2004, Dome structures in collision orogens: Mechanical investigation of the gravity/compression interplay, *in* Whitney, D.L., Teyssier, C., and Siddoway, C.S., eds., Gneiss Domes in Orogeny: Geological Society of America Special Paper 380, p. 47–66.

Burtman, V.S., 2000, Cenozoic crustal shortening between the Pamir and Tien Shan and a reconstruction of the Pamir–Tien Shan transition zone for the Cretaceous and Palaeogene: Tectonophysics, v. 319, p. 69–92, doi: 10.1016/S0040-1951(00)00022-6.

Burtman, V.S., and Molnar, P., 1993, Geological and geophysical evidence for deep subduction of continental crust beneath the Pamir: Geological Society of America Special Paper 281, 76 p.

Chung, S.-L., Chu, M.-F., Zhang, Y., Xie, Y., Lo, C.-H., Lee, T.-Y., Lan, C.-Y., Li, X., Zhang, Q., and Wang, Y., 2005, Tibetan tectonic evolution inferred from spatial and temporal variations in post-collisional magmatism: Earth-Science Reviews, v. 68, p. 173–196, doi: 10.1016/j.earscirev.2004.05.001.

Cowgill, E., Yin, A., Harrison, T.M., and Xiao-Feng, W., 2003, Reconstruction of the Altyn Tagh fault based on U-Pb geochronology: Role of back thrusts, mantle sutures, and heterogeneous crustal strength in forming the Tibetan Plateau: Journal of Geophysical Research, v. 108, no. B7, p. 2346, doi: 10.1029/2002JB002080.

Davis, G.A., and Lister, G.S., 1988, Detachment faulting in continental extension: Perspectives from the southwestern U.S. Cordillera, *in* Clark, S.P., Jr., Burchfiel, B.C., Suppe, J., eds., Processes in continental lithospheric deformation: Geological Society of America Special Paper 218, p. 133–159.

Ding, L., Zhong, D., Yin, A., Kapp, P., and Harrison, T.M., 2001, Cenozoic structural and metamorphic evolution of the eastern Himalayan syntaxis (Namche Barwa): Earth and Planetary Science Letters, v. 192, p. 423–438, doi: 10.1016/S0012-821X(01)00463-0.

Ducea, M.N., Lutkov, V., Minaev, V.T., Hacker, B., Ratschbacher, L., Luffi, P., Schwab, M., Gehrels, G.E., McWilliams, M., Vervoort, J., and Metcalf, J., 2003, Building the Pamirs: The view from the underside: Geology, v. 31, no. 10, p. 849–852, doi: 10.1130/G19707.1.

Fraser, J.E., Searle, M.P., Parrish, R.R., and Nobel, S.R., 2001, Chronology of deformation, metamorphism, and magmatism in the southern Karakoram Mountains: Geological Society of America Bulletin, v. 113, no. 11, p. 1443–1455, doi: 10.1130/0016-7606(2001)113<1443:CODMAM>2.0.CO;2.

Gaetani, M., 1997, The Karakorum block in Central Asia, from Ordovician to Cretaceous: Sedimentary Geology, v. 109, p. 339–359, doi: 10.1016/S0037-0738(96)00068-1.

Hacker, B., Luffi, P., Lutkov, V., Minaev, V., Ratschbacher, L., Plank, T., Ducea, M.N., Patiño-Douce, A.E., McWilliams, M., and Metcalf, J., 2005, Near-ultrahigh pressure processing of continental crust: Miocene crustal xenoliths from the Pamir: Journal of Petrology, v. 46, no. 8, p. 1661–1687, doi: 10.1093/petrology/egi030.

Haines, S.S., Klemperer, S.L., Brown, L., Jingru, G., Mechie, J., Meissner, R., Ross, A., and Wenjin, Z., 2003, INDEPTH III seismic data: From surface observations to deep crustal processes in Tibet: Tectonics, v. 22, no. 1, p. 1001, doi: 10.1029/2001TC001305,2003.

Horton, B.K., Yin, A., Spurlin, M.S., Zhou, J., and Wang, J., 2002, Paleocene-Eocene syncontractional sedimentation in narrow, lacustrine-dominated basins of east-central Tibet: Geological Society of America Bulletin, v. 114, no. 7, p. 771–786, doi: 10.1130/0016-7606(2002)114<0771:PESSIN>2.0.CO;2.

Hoskin, P.W.O., and Black, L.P., 2000, Metamorphic zircon formation by solid-state recrystallization of protolith igneous zircon: Journal of Metamorphic Geology, v. 18, p. 423–439, doi: 10.1046/j.1525-1314.2000.00266.x.

Houseman, G., and England, P., 1996, A lithospheric-thickening model for the Indo-Asian collision, *in* Yin, A., and Harrison, T.M., eds., The Tectonic Evolution of Asia: New York, Cambridge University Press, p. 3–17.

Hsu, K.J., Pan, G., and engör, A.M.C., 1995, Tectonic evolution of the Tibetan Plateau: A working hypothesis based on the archipelago model of orogenesis: International Geology Review, v. 37, p. 473–508.

Kapp, J.L.D.A., Harrison, T.M., Kapp, P., Grove, M., Lovera, O.M., and Lin, D., 2005, Nyainqentanglha Shan: A window into the tectonic, thermal, and geochemical evolution of the Lhasa block, southern Tibet: Journal of Geophysical Research, v. 110, no. B08413, doi: 10.1029/2004JB003330.

Kapp, P., Yin, A., Manning, C.E., Murphy, M., Harrison, T.M., and Spurlin, M., 2000, Blueschist-bearing metamorphic core complexes in the Qiangtang block reveal deep crustal structure of northern Tibet: Geology, v. 28,

no. 1, p. 19–22, doi: 10.1130/0091-7613(2000)28<19:BMCCIT>2.0.CO;2.

Kapp, P., Murphy, M.A., Yin, A., Harrison, T.M., Lin, D., and Jinghui, G., 2003a, Mesozoic and Cenozoic tectonic evolution of the Shiquanhe area of western Tibet: Tectonics, v. 22, 1029, doi: 10.1029/2001TC001332.

Kapp, P., Yin, A., Manning, C.E., Harrison, T.M., and Taylor, M., 2003b, Tectonic evolution of the early Mesozoic blueschist-bearing Qiangtang metamorphic belt, central Tibet: Tectonics, v. 22, no. 4, 1043, doi: 10.1029/2002TC001383.

Koziol, R., and Newton, R.C., 1988, Redetermination of the anorthite breakdown reaction and improvement of the plagioclase-garnet Al_2SiO_5-quartz geobarometer: The American Mineralogist, v. 73, p. 216–223.

Lacassin, R., Valli, F., Arnaud, N., Leloup, P.H., Papuette, J.L., Haibing, L., Tapponnier, P., Chevalier, M.-L., Guillot, S., Mahéo, G., and Zhiqin, X., 2004, Large-scale geometry, offset and kinematic evolution of the Karakorum fault, Tibet: Earth and Planetary Science Letters, v. 219, p. 255–269, doi: 10.1016/S0012-821X(04)00006-8.

Leier, A.L., DeCelles, P.G., Kapp, P., and Ding, L., 2007, The Takena Formation of the Lhasa terrane, southern Tibet: The record of a Late Cretaceous retroarc foreland basin: Geological Society of America Bulletin, v. 119, no. 1/2, p. 31–48, doi: 10.1130/B25974.1.

Lister, G.S., and Davis, G.A., 1989, The origin of metamorphic core complexes and detachment faults formed during Tertiary continental extension in the northern Colorado River region, U.S.A.: Journal of Structural Geology, v. 11, p. 65–94, doi: 10.1016/0191-8141(89)90036-9.

Liu, Z.Q., 1988, Geologic Map of the Qinghai-Xizang Plateau and its Neighboring Regions: Beijing, Chengdu Institute of Geology and Mineral Resources, Geological Publishing House, scale 1:5,000,000.

Ludwig, K.R., 2003, Users' Manual for Isoplot/Ex Version 3.0: A Geochronological Toolkit for Microsoft Excel: Berkeley, Berkeley Geochronology Center Special Publication 4, 70 p.

Mahéo, G., Pêcher, A., Guillot, S., Rolland, Y., and Delacourt, C., 2004, Exhumation of Neogene domes between oblique crustal boundaries in south Karakorum (northwest Himalaya, Pakistan), *in* Whitney, D.L., Teyssier, C., and Siddoway, C.S., eds., Gneiss Domes in Orogeny: Geological Society of America Special Paper 380, p. 141–154.

Matte, P., Tapponnier, P., Arnaud, N., Bourjot, L., Avouac, J.P., Vidal, P., Liu, Q., Pan, Y., and Wang, Y., 1996, Tectonics of Western Tibet, between the Tarim and the Indus: Earth and Planetary Science Letters, v. 142, p. 311–330, doi: 10.1016/0012-821X(96)00086-6.

Mojzsis, S.J., and Harrison, T.M., 2002, Establishment of a 3.83-Ga magmatic age for the Akilia tonalite (southern West Greenland): Earth and Planetary Science Letters, v. 202, p. 563–576, doi: 10.1016/S0012-821X(02)00825-7.

Murphy, M.A., Yin, A., Harrison, T.M., Durr, S.B., Chen, Z., Ryerson, F.J., Kidd, W.S.F., Wang, X., and Zhou, X., 1997, Did the Indo-Asian collision alone create the Tibetan Plateau?: Geology, v. 25, p. 719–722, doi: 10.1130/0091-7613(1997)025<0719:DTIACA>2.3.CO;2.

Murphy, M.A., Yin, A., Kapp, P., Harrison, T.M., Ling, D., and Jinghui, G., 2000, Southward propagation of the Karakoram fault system, southwest Tibet: Timing and magnitude of slip: Geology, v. 28, no. 5, p. 451–454, doi: 10.1130/0091-7613(2000)28<451:SPOTKF>2.0.CO;2.

Neil, E.A., and Houseman, G.A., 1997, Geodynamics of the Tarim Basin and the Tian Shan in central Asia: Tectonics, v. 16, no. 4, p. 571–584, doi: 10.1029/97TC01413.

Pan, Y., 1992, Introduction to Integrated Scientific Investigation on Karakoram and Kunlun Mountains: Beijing, China Meteorological Press, 92 p.

Pan, Y., and Bian, Q., 1996, Tectonics, *in* Pan, Y., ed., Geological Evolution of the Karakoram and Kunlun Mountains: Beijing, Seismological Press, p. 187–229.

Pashkov, B.R., and Dmitriyev, E.A., 1982, Muzkol' crystalline massif (Central Pamir): International Geology Review, v. 24, no. 3, p. 285–296.

Peltzer, G., and Tapponnier, P., 1988, Formation and evolution of strike-slip faults, rifts, and basins during the India-Asia collision: An experimental approach: Journal of Geophysical Research, v. 93, p. 15,085–15,117.

Peykre, Y.B., Ye, A.P., and Zotov, I.A., 1982, The Muzkol' metamorphic complex of the Central Pamir: International Geology Review, v. 24, no. 3, p. 297–303.

Powell, R., Holland, T., and Worley, B., 1998, Calculating phase diagrams involving solid solutions via non-linear equations, with examples using THERMOCALC: Journal of Metamorphic Geology, v. 116, no. 4, p. 557–588.

Ratschbacher, L., Frisch, W., Liu, G., and Chen, C.C., 1994, Distributed deformation in southern and western Tibet during and after the India-Asian collision: Journal of Geophysical Research, v. 99, p. 19,917–19,945, doi: 10.1029/94JB00932.

Robinson, A.C., Yin, A., Manning, C.E., Harrison, T.M., Zhang, S.-H., and Wang, X.-F., 2004, Tectonic evolution of the northeastern Pamir: Constraints from the northern portion of the Cenozoic Kongur Shan extensional system: Geological Society of America Bulletin, v. 116, p. 953–974, doi: 10.1130/B25375.1.

Robinson, A.C., Yin, A., and Lovera, O.M., 2005, Thermokinematic modeling of the effect of footwall erosion on cooling age patterns in detachment fault settings: Eos (Transactions, American Geophysical Union), v. 86, no. 52, p. 243.

Schwab, M., Ratschbacher, L., Siebel, W., McWilliams, M., Minaev, V., Lutkov, V., Chen, F., Stanek, K., Nelson, B., Frisch, W., and Wooden, J.L., 2004, Assembly of the Pamirs: Age and origin of magmatic belts from the southern Tien Shan to the southern Pamirs and their relation to Tibet: Tectonics, v. 23, TC4002, doi: 10.1029/2003TC001583.

Searle, M.P., 1996, Geological evidence against large-scale pre-Holocene offsets along the Karakoram fault: Implications for the limited extrusion of the Tibetan Plateau: Tectonics, v. 15, no. 1, p. 171–186, doi: 10.1029/95TC01693.

Searle, M.P., Weinberg, R.F., and Dunlap, W.J., 1998, Transpressional tectonics along the Karakoram fault zone, northern Ladakh: Constraints on Tibetan extrusion, *in* Holdsworth, R.E., Strachan, R.A., and Dewey, J.F., eds., Continental Transpressional and Transtensional Tectonics: Geological Society of London Special Publication 135, p. 307–326.

Şengör, A.M.C., and Natal'in, B.A., 1996, Paleotectonics of Asia: Fragments of a synthesis, *in* Yin, A., and Harrison, T.M., eds., The Tectonic Evolution of Asia: New York, Cambridge University Press, p. 486–640.

Şengör, A.M.C., and Okurogullari, A.H., 1991, The role of accretionary wedges in the growth of continents: Asiatic examples from Argand to plate tectonics: Eclogae Geologicae Helvetiae, v. 84, no. 3, p. 535–597.

Sobel, E.R., and Dumitru, T.A., 1997, Thrusting and exhumation around the margins of the western Tarim Basin during the India-Asia collision: Journal of Geophysical Research, v. 102, no. B3, p. 5043–5063, doi: 10.1029/96JB03267.

Spurlin, M.S., Yin, A., Horton, B.K., Zhou, J., and Wang, J., 2005, Structural evolution of the Yushu-Nanqian region and its relationship to syncollisional igneous activity, east-central Tibet: Geological Society of America Bulletin, v. 117, no. 9/10, p. 1293–1317, doi: 10.1130/B25572.1.

Strecker, M.R., Frisch, W., Hamburger, M.W., Ratschbacher, L., Semiletkin, S., Zamoruyev, A., and Sturchio, N., 1995, Quaternary deformation in the Eastern Pamirs, Tadzhikistan and Kyrgyzstan: Tectonics, v. 14, no. 5, p. 1061–1079, doi: 10.1029/95TC00927.

Tapponnier, P., Mattauer, M., Proust, F., and Cassaigneau, C., 1981, Mesozoic ophiolites, sutures, and large-sale tectonic movements in Afghanistan: Earth and Planetary Science Letters, v. 52, p. 355–371, doi: 10.1016/0012-821X(81)90189-8.

Tapponnier, P., Peltzer, G., Le Dain, A.Y., Armijo, R., and Cobbold, P., 1982, Propagating extrusion tectonics in Asia: New insights from simple experiments with plasticine: Geology, v. 10, p. 611–616, doi: 10.1130/0091-7613(1982)10<611:PETIAN>2.0.CO;2.

Taylor, M., Yin, A., Ryerson, F.J., Kapp, P., and Ding, L., 2003, Conjugate strike-slip faulting along the Bangong-Nujiang suture zone accommodates coeval east-west extension and north-south shortening in the interior of the Tibetan Plateau: Tectonics, v. 22, no. 4, p. 1044, doi: 10.1029/2002TC001361.

Teyssier, C., and Whitney, D.L., 2002, Gneiss domes and orogeny: Geology, v. 30, no. 12, p. 1139–1142, doi: 10.1130/0091-7613(2002)030<1139:GDAO>2.0.CO;2.

Thomas, J.-C., Chauvin, A., Gapais, D., Bazhenov, M.L., Perroud, H., Cobbold, P.R., and Burtman, V.S., 1994, Paleomagnetic evidence for Cenozoic block rotations in the Tadjik depression (Central Asia): Journal of Geophysical Research, v. 99, no. B8, p. 15,141–15,160, doi: 10.1029/94JB00901.

Thomas, J.-C., Cobbold, P.R., Wright, A., and Gapais, D., 1996, Cenozoic tectonics of the Tadzhik depression, Central Asia, *in* Yin, A., and Harrison, T.M., eds., The Tectonic Evolution of Asia: New York, Cambridge University Press, p. 191–207.

Waldhör, M., Appel, E., Frisch, W., and Patzelt, A., 2001, Palaeomagnetic investigation in the Pamirs and its tectonic implications: Journal of Asian Earth Sciences, v. 19, p. 429–451, doi: 10.1016/S1367-9120(00)00030-4.

Wernicke, B., and Axen, G.J., 1988, On the role of isostasy in the evolution of normal fault systems: Geology, v. 16, p. 848–851, doi: 10.1130/0091-7613(1988)016<0848:OTROII>2.3.CO;2.

Whitney, D.L., Teyssier, C., and Vanderhaeghe, O., 2004, Gneiss domes and crustal flow, *in* Whitney, D.L., Teyssier, C., and Siddoway, C.S., eds., Gneiss Domes in Orogeny: Geological Society of America Special Paper 380, p. 15–33.

Xiao, W.J., Windley, B.F., Chen, H.L., Zhang, G.C., and Li, J.L., 2002, Carboniferous-Triassic subduction and accretion in the western Kunlun, China: Implications for the collisional and accretionary tectonics of the northern Tibetan Plateau: Geology, v. 30, no. 4, p. 295–298, doi: 10.1130/0091-7613(2002)030<0295:CTSAAI>2.0.CO;2.

Xinjiang Bureau of Geology and Mineral Resources, 1993, Regional Geology of Xinjiang Uygur Autonomous Region: Beijing, Geological Publishing House, 841 p. (in Chinese with English abstract).

Xu, R., Zhang, Y., Xie, Y., Vidal, P., Arnaud, N., Zhang, Q., and Zhao, D., 1996, Isotopic geochemistry of plutonic rocks, *in* Pan, Y., ed., Geological Evolution of the Karakoram and Kunlun Mountains: Beijing, Seismological Press, p. 137–186.

Yin, A., and Harrison, T.M., 2000, Geologic Evolution of the Himalayan-Tibetan orogen: Annual Review of Earth and Planetary Sciences, v. 28, p. 211–280, doi: 10.1146/annurev.earth.28.1.211.

Yin, A., and Nie, S., 1996, A Phanerozoic palinspastic reconstruction of China and its neighboring regions, *in* Yin, A., and Harrison, T.M., eds., The Tectonic Evolution of Asia: New York, Cambridge University Press, p. 442–485.

Yin, A., Robinson, A., and Manning, C.E., 2001, Oroclinal bending and slab break-off causing coeval east-west extension and east-west contraction in the Pamir–Nanga Parbat syntaxis in the past 10 m.y.: Eos (Transactions, American Geophysical Union), v. 82, no. 47, p. F1124.

Yin, A., Rumelhart, P.E., Butler, R., Cowgill, E., Harrison, T.M., Foster, D.A., Ingersoll, R.V., Qing, Z., Xian-Qiang, Z., Xiao-Feng, W., Hanson, A., and Raza, A., 2002, Tectonic history of the Altyn Tagh fault system in northern Tibet inferred from Cenozoic sedimentation: Geological Society of America Bulletin, v. 114, no. 10, p. 1257–1295, doi: 10.1130/0016-7606(2002)114<1257:THOTAT>2.0.CO;2.

Yin, J., and Bian, Q., 1992, Geologic Map of the Karakoram–Western Kunlun and Adjacent Regions: Beijing, Science Press, scale 1:2,000,000.

Youngun, Y., and Hsu, K.J., 1994, Origin of the Kunlun Mountains by arc-arc and arc-continent collisions: The Island Arc, v. 3, no. 2, p. 75–89, doi: 10.1111/j.1440-1738.1994.tb00096.x.

Zhang, Y., Xie, Y., Xu, R., Vidal, P., and Arnaud, N., 1996, Geochemistry of granitoid rocks, *in* Pan, Y., ed., Geological Evolution of the Karakoram and Kunlun Mountains: Beijing, Seismological Press, p. 94–136.

Manuscript Received 27 January 2006
Revised Manuscript Received 16 January 2007
Manuscript Accepted 19 January 2007

Printed in the USA

Cenozoic evolution of the eastern Pamir: Implications for strain-accommodation mechanisms at the western end of the Himalayan-Tibetan orogen
Alexander C. Robinson, An Yin, Craig E. Manning, T. Mark Harrison, Shuan-Hong Zhang, Xiao-Feng Wang
Supplement to: *Geological Society of America Bulletin*, v. 119, no. 7/8, doi: 10.1130/B25981.S1.
Figures 4 and 5

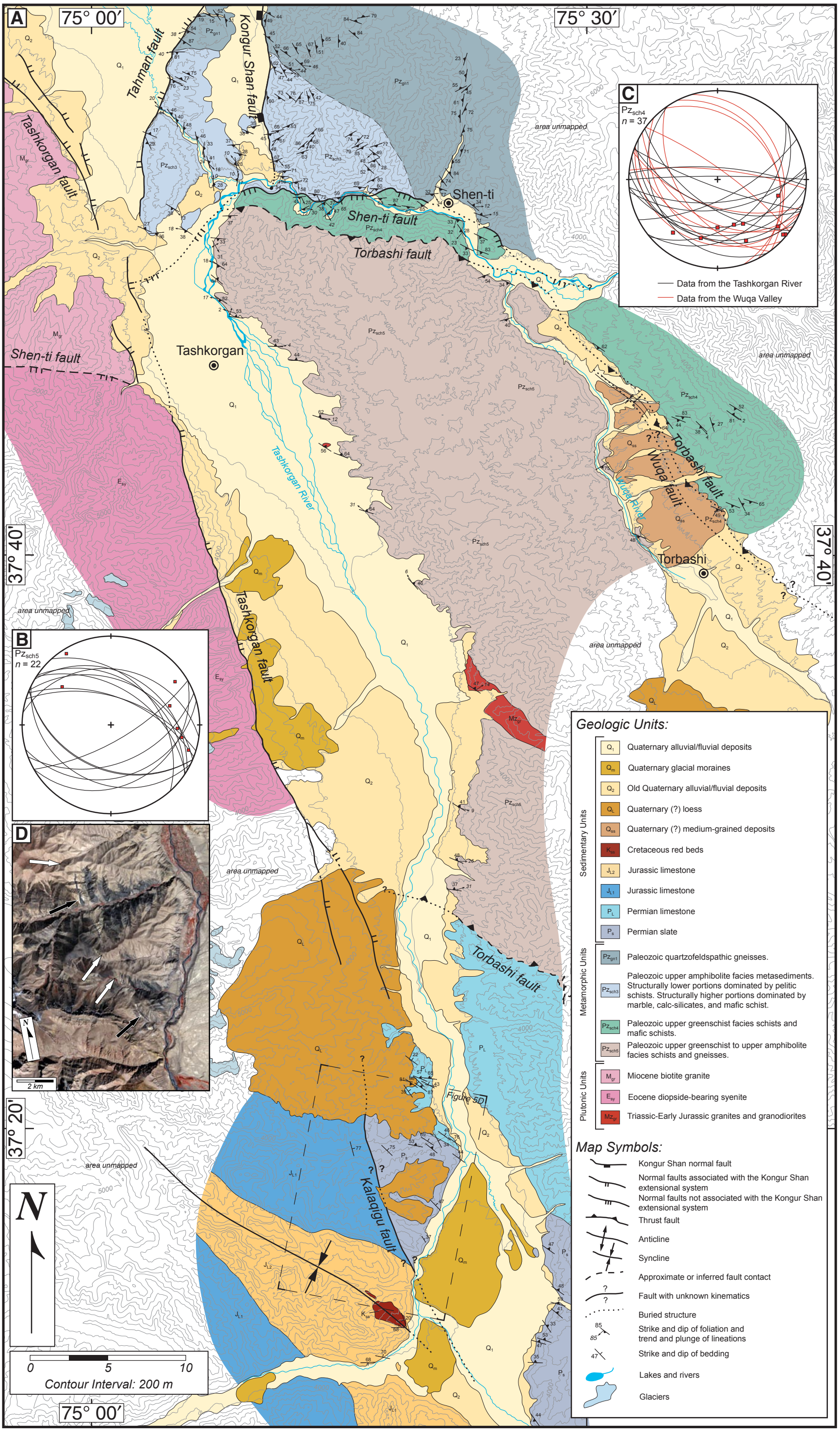

Figure 4. (A) Geologic map of the Tashkorgan normal fault, NE Pamir, China. Lower-hemisphere equal-area stereonets show foliation planes and lineations from (B) unit Pzsch4, and (C) unit Pzsch5. (D) ASTER (Advanced Spaceborne Thermal Emission and Reflection Radiometer) visible bands (red—3; green—2; blue—1) of the Kalaqigu fault (black arrows) south of the Tashkorgan fault. Undisturbed Quaternary deposits capping ridges (white arrows) indicate no recent motion along the fault.

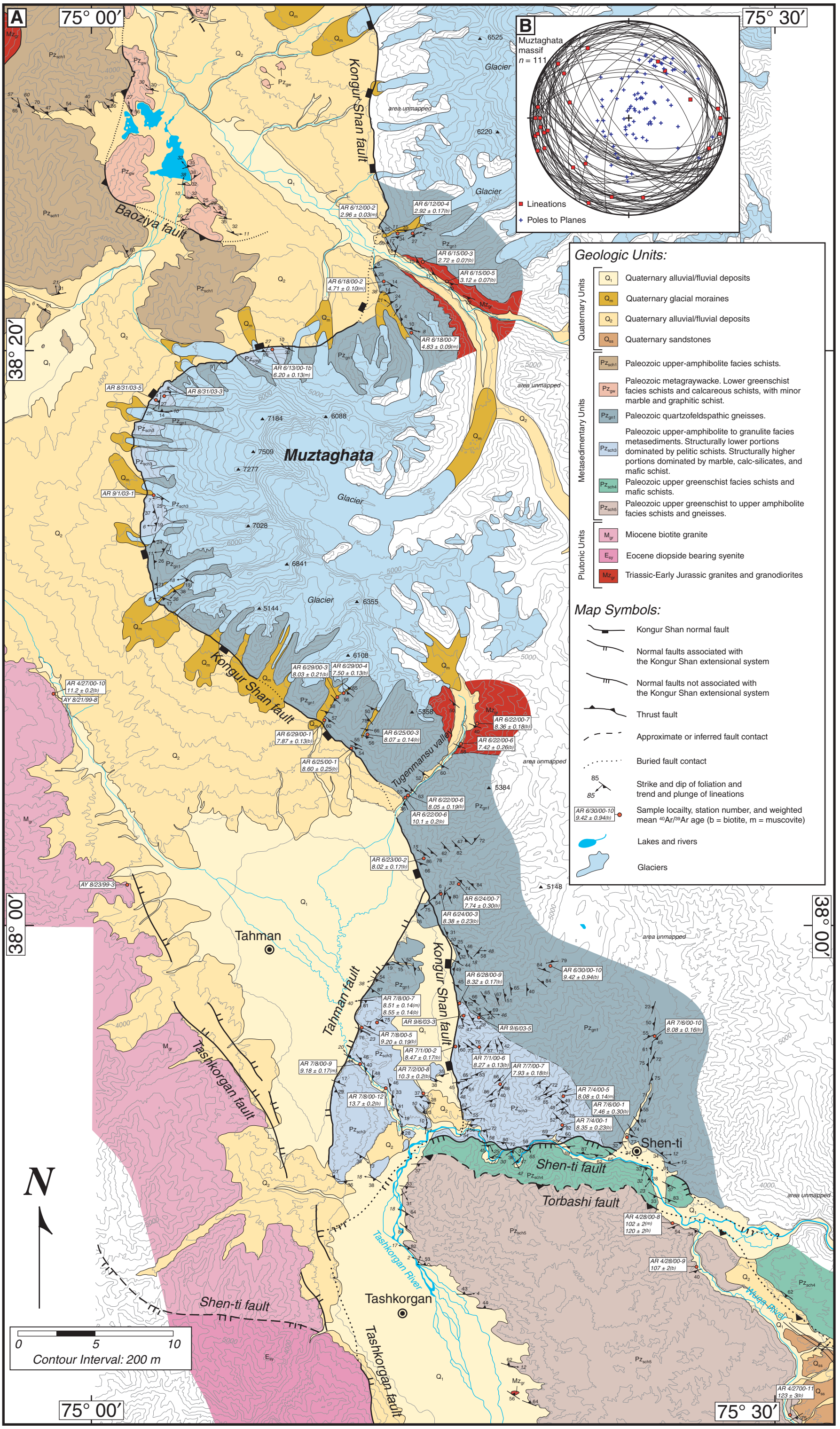

Figure 5. (A) Geologic map of the southern Kongur Shan normal fault. (B) Lower-hemisphere equal-area stereonet showing foliation planes (black lines), poles to planes (blue crosses), and lineations (red squares) from the Muztaghata massif.